

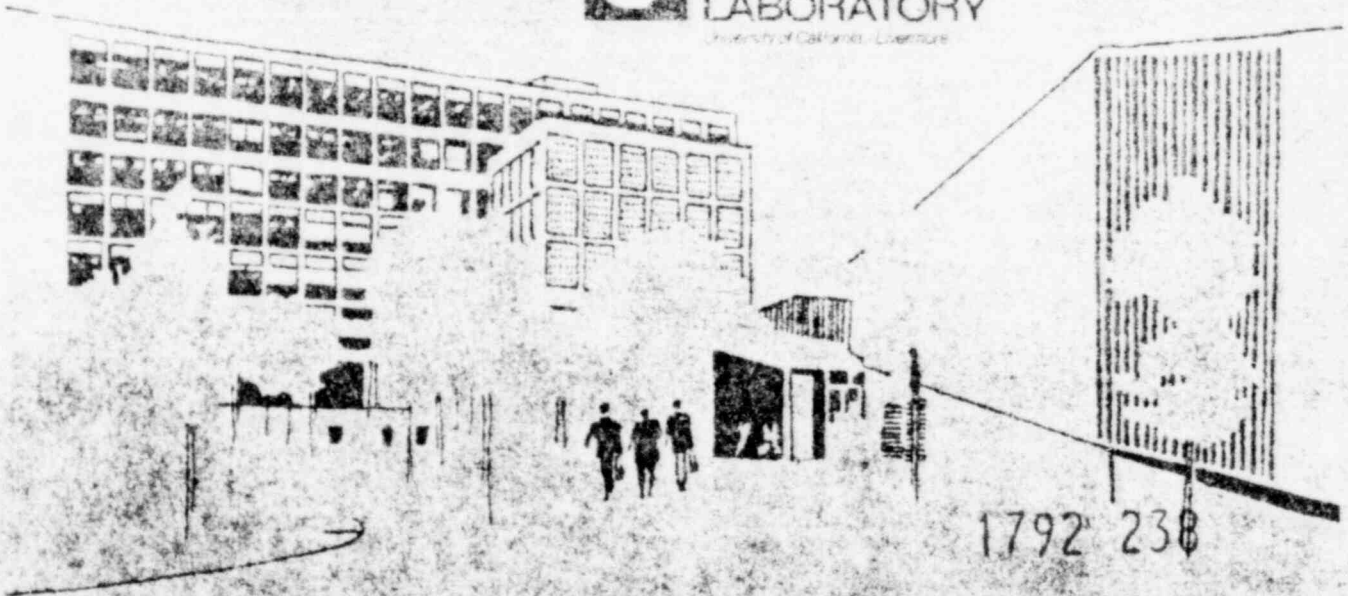
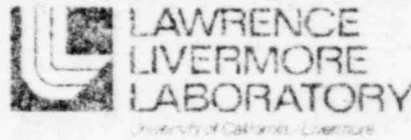
SEISMIC ANALYSIS OF THE ACID LIQUID WASTE TANKS AT THE WESTERN NEW YORK STATE NUCLEAR SERVICE CENTER, WEST VALLEY, NEW YORK

POOR ORIGINAL

C. Y. Liaw
A. M. Davito
R. C. Murray

March 1979

This work was supported by the U.S. Nuclear Regulatory Commission under Interagency Agreement DOE 40-550-75 with the U.S. Department of Energy.





LAWRENCE LIVERMORE LABORATORY

University of California / Livermore, California, 94550

UCRL-52600

SEISMIC ANALYSIS OF THE ACID LIQUID
WASTE TANKS AT THE WESTERN
NEW YORK STATE NUCLEAR SERVICE CENTER,
WEST VALLEY, NEW YORK

C. Y. Liaw

A. M. Davito

R. C. Murray

EG&G, Inc., San Ramon, CA

MS. date: March 1979

1792 239

CONTENTS

Abstract	v11
Introduction	1
Summary	3
Structural Review	3
Analysis Technique	3
Structural Models	3
Structural Loading	4
Analyses	4
Limiting Criteria	5
Interpretation of Results	6
Tank	6
Vault	6
Facility Description	9
Mathematical Model	13
Tank Analysis	14
Tank Model	14
Structural Loading	16
Static Loads	16
Seismic Loads	16
Seismic Analysis Method	21
Combination of Loads	21
Limiting Criteria	22
Results	24
Vault Analysis	26
Vault Model	26
Structural Loading	27
Static Load	27
Seismic Load	28
Seismic Analysis Method	33
Combination of Loads	33

Limiting Criteria	33
Results	35
Conclusions	43
Acknowledgment	45
References	46
Appendix: Calculation of the Maximum Temperature Differential Through the Vault Walls	48

045 SEP 77

1792 241

LIST OF ILLUSTRATIONS

1. Location of acid liquid-waste tanks 8D-3 and 8D-4	10
2. Storage tanks 8D-3 and 8D-4 and the reinforced concrete vault and liner	11
3a. Close-up of tank leg support assembly	12
3b. Plan view of base plate geometry	12
4. Tank finite element model	15
5. Horizontal (a) and vertical (b) response spectra from NRC Regulatory Guide 1.60	17
6. Hydrodynamic pressure, P , resulting from a small impulsive excitation, a , on the inside wall of a rigid cylinder	20
7. Finite element model of vault	27
8a. Bending moments, M , that result from positive pressure acting on the left side of the vault (shown in cross section)	30
8b. Bending moments that result from negative pressure acting on the right side of the vault	31
8c. Combined bending moments resulting from positive pressure on one side of the vault and negative pressure on the other side	32
9. Methods used to combine the seven basic static analyses in Table 2	36
10. Regions of vault model where limiting criteria are exceeded with 25% of the base thermal load included in the analysis	39
11. Regions of vault model where limiting criteria are exceeded with 50% of the base thermal load	40
12. Regions of vault model where limiting criteria are exceeded with 75% of the base thermal load	41
13. Regions of vault model where limiting criteria are exceeded with 100% of the base thermal load	42

A1. Planar vault and control surface used for flux plot method	50
A2. Flux plot for a corner of the planar vault.	50
A3. Vault, control volume, and geometric parameters for three-dimensional approach	52

LIST OF TABLES

1. Limiting peak accelerations and locations for the vault model	8
2. Seven basic static analyses of vault and scaling factors used to account for different peak accelerations	35
A1. Results of flux plot calculations for T_2 and ΔT	51

SAS SP11

ABSTRACT

This report was prepared at the request of the Nuclear Regulatory Commission as part of a review of the nuclear fuel reprocessing plant operated by Nuclear Fuel Services, Inc., at West Valley, N.Y. The report discusses the seismic evaluation by Lawrence Livermore Laboratory of two high-level, acid liquid-waste tanks, 8D-3 and 8D-4, adjacent to the plant. It describes the tanks and discusses the techniques used to model and analyze the structures and to combine the loads. Limiting criteria, results, and conclusions are presented.

INTRODUCTION

The Nuclear Regulatory Commission (NRC) asked the Lawrence Livermore Laboratory (LLL) to assess the seismic integrity of the reprocessing facility operated by Nuclear Fuel Services, Inc., (NFS) at West Valley, N. Y. The assessment began with a seismic analysis of the process building.^{1,2} Next, we analyzed the neutralized liquid-waste tanks located north of the building and the fuel receiving station adjacent to the process building.^{3,4} This report presents our analysis of two high-level, acid liquid-waste tanks located next to the neutralized liquid-waste tanks.

One of the acid waste tanks (8D-3) is a spare. The other identical tank (8D-4) is full and contains 12,000 gal of high-level acid liquid waste generated by reprocessing spent nuclear fuel. Each tank is 12 ft in diameter and 15.75 ft in height and is made of 304L stainless steel. External supports, reinforcement, and piping are either 304 or 304L stainless steel. Each tank is supported by vertical legs made of 8-in. extra strong pipe. The lower end of each leg is welded to a base plate that is secured by two bolts to the foundation.

The tanks sit inside a vault that is basically a rectangular reinforced concrete box buried 6 ft underground. Stainless steel, 1/8-in. thick, lines the floor and the inside vault wall to a height of 1.5 ft, creating a pan under the tanks.

The seismic analysis identified the ground acceleration (up to 0.2 g) that the tanks and vault could withstand before limiting criteria were exceeded. Limiting criteria define the level of stress, deflection, or degradation that initiates structural distress. Known conservatism was removed from the analysis to achieve a realistic assessment of integrity.

845 SP77

We took the following steps to assess both the current and future seismic safety of the tanks and vault:

- Reviewed details of tanks and vault
- Selected analysis technique
- Selected structural modeling technique
- Selected structural loading
- Performed the analyses
- Developed limiting criteria
- Interpreted results
- Drew conclusions.

We used our judgment extensively throughout the project to make modeling decisions and to select limiting criteria. We relied on past experience, published literature, and discussions with the NRC in making these decisions.

245 SPT

SUMMARY

We performed a seismic analysis of two identical stainless steel liquid-waste tanks, 8D-3 and 8D-4, and the reinforced concrete vault in which they rest. The tanks are located adjacent to the Nuclear Fuel Reprocessing Plant operated by Nuclear Fuel Services, Inc., at the Western New York State Nuclear Service Center near West Valley, N. Y.

The analysis was done at the request of the NRC to determine whether the tanks and vault could survive, without structural distress, an earthquake with peak acceleration of up to 0.2 g.

STRUCTURAL REVIEW

We familiarized ourselves with the structures by reviewing drawings supplied by NFS through the NRC.

ANALYSIS TECHNIQUE

The tank analysis consisted of static analyses of working loads and a dynamic analysis of seismic loads using the response-spectrum method. The vault analysis also considered both static and dynamic loads. We treated dynamic loads, including the inertial load of the structure and the dynamic soil pressure, as equivalent static loads. This approach gives good results for stiff structures.

STRUCTURAL MODELS

Because there is practically no tank-vault interaction, separate finite element models were developed for the structures, and the analyses proceeded independently. Symmetry considerations allowed simple mathematical models. Because of tank symmetry, only one-fourth of the tank had to be modeled. Likewise, only half the vault was modeled.

Only the tank containing waste was modeled. Its dome-shaped roof, cylindrical shell wall, and flat bottom plate were modeled using quadrilateral plate/shell elements of the SAP4 computer code.⁵ Radial and transverse stiffeners and vertical legs were modeled using beam elements.

The walls and roof of the vault were modeled using plate/shell elements, and the walls were assumed fixed at the base. Six horizontal girders in the roof were modeled by beam elements.

STRUCTURAL LOADING

Structural loading included dead load, thermal load, hydrostatic load, and seismic loads. At the request of the NRC, earthquakes having up to 0.2-g peak horizontal ground acceleration were considered. The response spectrum presented in Regulatory Guide 1.60⁶ was used as the free-field input ground motion for the response-spectrum analysis of the tank. A damping ratio of 0.01 was used to account for the liquid waste in the tank.

Operating loads for the vault consisted of the dead weight of the vault, the weight of the tanks, liquid waste, and other equipment, and the weight of the 6 ft of overburden.

ANALYSES

Linear elastic analyses were conducted using both static and response-spectrum techniques to evaluate the behavior of a tank and its stored liquid waste during an earthquake. Static and seismic loads were combined.

A linear elastic static analysis of the vault was conducted. Dynamic soil pressure was estimated to be the equivalent static pressure, which was calculated using the Mononobe-Okabe theory.^{7,8} Two methods were used to combine static and dynamic loads.

LIMITING CRITERIA

The basic consideration for evaluating the tank performance was its ability to confine the liquid waste. Limiting criteria for the tank were developed for the following three critical cases:

- Yielding or buckling of the shell wall
- Yielding of the bottom plate
- Yielding or buckling of the support legs and stiffeners.

For shell members and the bottom plate, limiting criteria were considered to be exceeded when calculated Von Mises stress for an element was greater than the yield stress of the steel. The critical buckling stress of a cylindrical shell under uniaxial compression was calculated. The value of 17.5 ksi was used as the critical buckling stress and analysis results were compared to it for each element of the shell.

The basic consideration for evaluating vault performance was its ability to provide secondary confinement of the waste. The limiting criterion was the one developed for a previous study of a buried reinforced concrete structure.³ The limiting criterion relates the actual loads and the calculated ultimate load capacities as follows:

$$\frac{P}{P_u} + \frac{V}{V_u} + \frac{M}{M_u} + \frac{T}{T_u} \leq 1.0$$

where the element resultant forces are defined as

P = axial force

V = shear force

M = bending moment

T = twisting moment

and the subscript "u" designates the ultimate quantities calculated using principles embodied in the ACI code.

1792 249

INTERPRETATION OF RESULTS

TANK

Results from the analyses were compared with limiting criteria and the following conclusions were drawn:

- All components of the tank model except the base plates of the support legs had stresses below the limiting stresses when subjected to 0.2-g peak ground acceleration. These stresses, expressed as a percentage of the limiting stresses, are as follows:

Support bolts:	<45%
Support legs:	<75%
Bottom plate stiffeners:	<50%
Bottom plate:	<25%
Shell wall:	<50%.

- Stress in the base plate exceeded the limiting stress at 0.16-g peak ground acceleration. At 0.2 g, the bending stress is 31 ksi (yield stress of plate = 25 ksi). This stress level would cause part of the base plate to yield but would not affect the function of the support leg.
- Maximum compressive stresses at 0.2 g were less than 20% of the critical buckling stress in the shell wall.

VAULT

Without a thermal load, limiting criteria for the vault are not exceeded for a peak ground acceleration of 0.2 g. With a thermal load, however, structural responses from the analysis of the concrete vault are consistent with previous studies of the NFS facilities,^{1,4} mainly, that bending moments induced by the estimated thermal gradient of 70°F in the walls and roof far exceed the ultimate moment capacities of the concrete section.

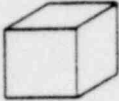
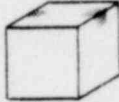
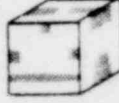


The fact that the vault still exists and shows little structural damage suggests that the thermal load was overestimated in the analysis. Two reasons may account for this: the gradient may actually be less than 70°F, or the thermal loads may have been relieved by the mechanisms of creep and crack formation in the concrete.

Accordingly, we examined five cases for which the thermal load was 0, 25, 50, 75, and 100% of the thermal load for a gradient of 70°F. Analysis results may be interpreted as cases with thermal gradients of 0°, 17.5°, 35°, 42.5°, and 70°F, respectively, and no stress relief, or as cases with a 70°F thermal gradient and varying degrees of stress relief. Results of these calculations appear in Table 1.

The actual residual thermal stresses in the concrete vault cannot be determined in this study because of the nonlinear behavior of reinforced concrete and because we have insufficient knowledge of the actual thermal gradient through the roof and walls. Until a nonlinear analysis of the vault is done, we must rely on our best engineering judgment to estimate the actual thermal stress in the vault and the peak ground acceleration that the vault can sustain. We believe that the actual thermal gradient is less than 70°F because the inside vault temperature built up over a long period of time. We also believe that some of the thermal load has relieved itself.

Based on these considerations, the 25% thermal load case is our best estimate of the actual thermal stress in the vault. For this case, limiting criteria are exceeded at only a few places near the center of the structure at 0.2-g peak ground acceleration.

TABLE 1. Limiting peak accelerations and locations for the vault model.
(For details see Figs. 10 to 13.)

Thermal load (% of load for 70°F thermal gradient)	Location where limiting criteria are exceeded	Acceleration at which limiting criteria exceeded, g
0		Not exceeded
25		0.18 to 0.2
50		0.04 near center, 0.12 to 0.16 elsewhere
75		0.02 roof
100		0.02

Our best estimate of the actual thermal load was submitted to the NRC in a review draft of this report. The NRC then asked that an additional study be done to confirm the use of the 25% thermal load case. This additional study estimated the maximum steady-state temperature gradient through the vault walls. Two approaches were used as explained in the Appendix. The maximum temperature differential was calculated to be 25.5°F, and results from the two methods agreed closely. This separate analysis confirms our selection of the 25% thermal load case as representative of the actual thermal gradient through the vault walls.

FACILITY DESCRIPTION

The waste storage facility for thorium bearing waste is located next to the neutralized waste storage facility north of the NFS process building (Fig. 1). The facility stores high-level liquid waste that was generated during reprocessing of fuel from Core A of Consolidated Edison's Indian Point No. 1 reactor. The acid waste storage system maintains the waste in an acidic medium to minimize thorium precipitation. The temperature is maintained at less than 140⁰F. The complex is designed for an average physical lifetime of not less than 50 years of active use. The design lifetime of the appurtenances and auxiliary equipment within the facility is 30 years.

Storage tank 8D-4 and its spare, 8D-3, are similar in construction (Fig. 2). The tanks are 12 ft in diameter and 15.75 ft in height with a nominal capacity of 15,000 gal. The tanks were fabricated of 304L stainless steel. External supports, bottom structural reinforcement, and piping are either 304 or 304L stainless steel. The tanks have a corrosion allowance of 0.07 in. A nozzle connection is provided for the insertion of corrosion coupons and for obtaining samples of the stored solution. The tanks are designed for a working volume of 13,500 gal each (90% of nominal capacity). Tank 8D-4 contains about 12,000 gal of waste.

The waste tanks are inside a reinforced concrete vault. The vault outside dimensions are 32 ft by 19 ft by 25.25 ft high. The vault floor is 41 ft by 28 ft. The vault walls are 1.75 ft thick. A 1/8-in. thick 304L stainless steel liner covers the floor and lines the inside vault wall to a height of 1.5 ft, creating a pan under the tanks. The area excavated for the vault was backfilled to a minimum overhead depth of 6 ft to provide a complete blanket of impermeable silty clay around the tank-vault complex as a barrier to potential leakage.

Each tank leg is made of 3-in.-diam. extra strong pipe welded to a base plate. The base plate is bolted to a support assembly that is anchored in the vault floor (Fig. 3).

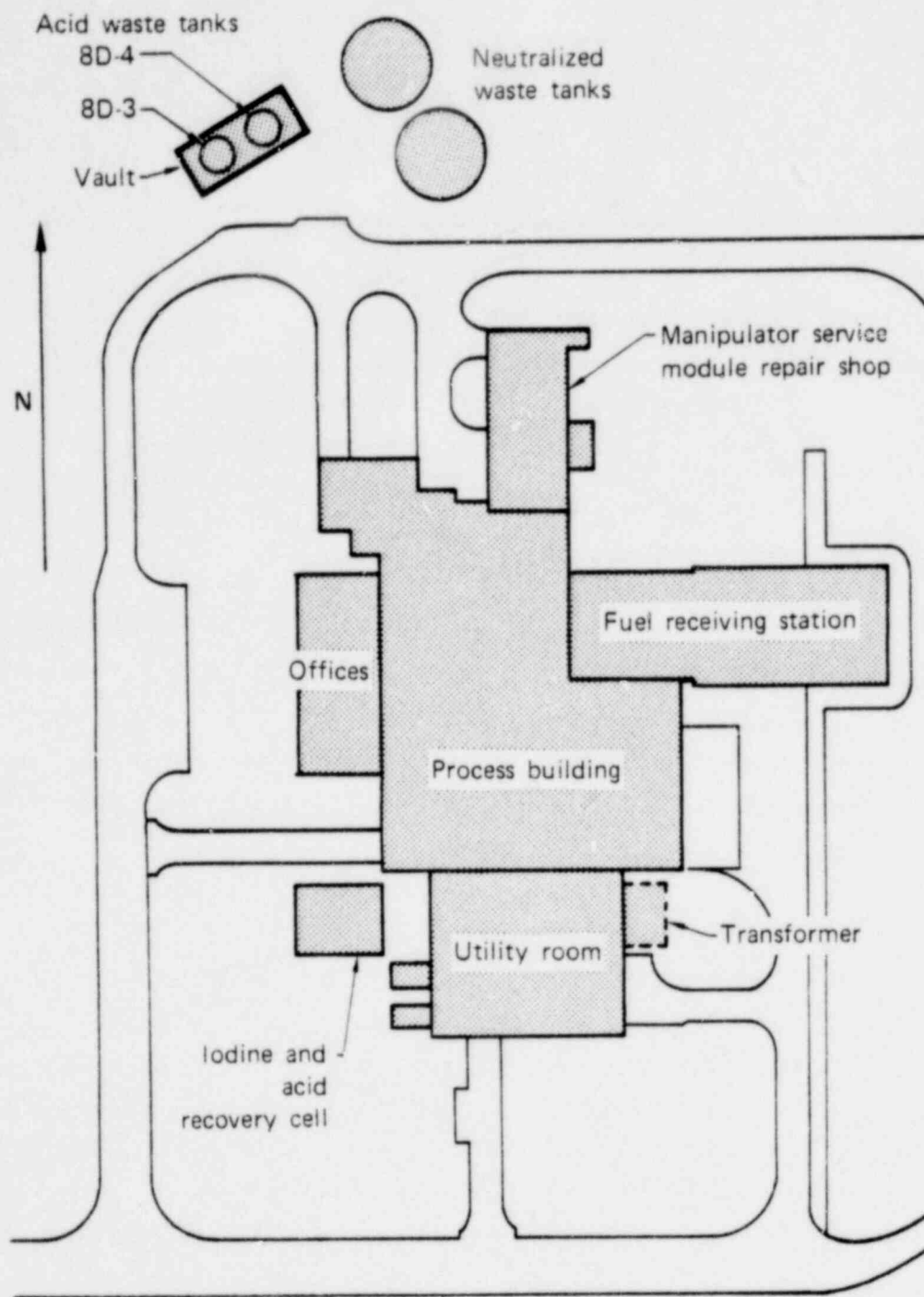


FIG. 1. Location of acid liquid-waste tanks 8D-3 and 8D-4 with respect to the nuclear fuel reprocessing plant operated by Nuclear Fuel Services, Inc., near West Valley, N. Y.

1792 254

MS 801

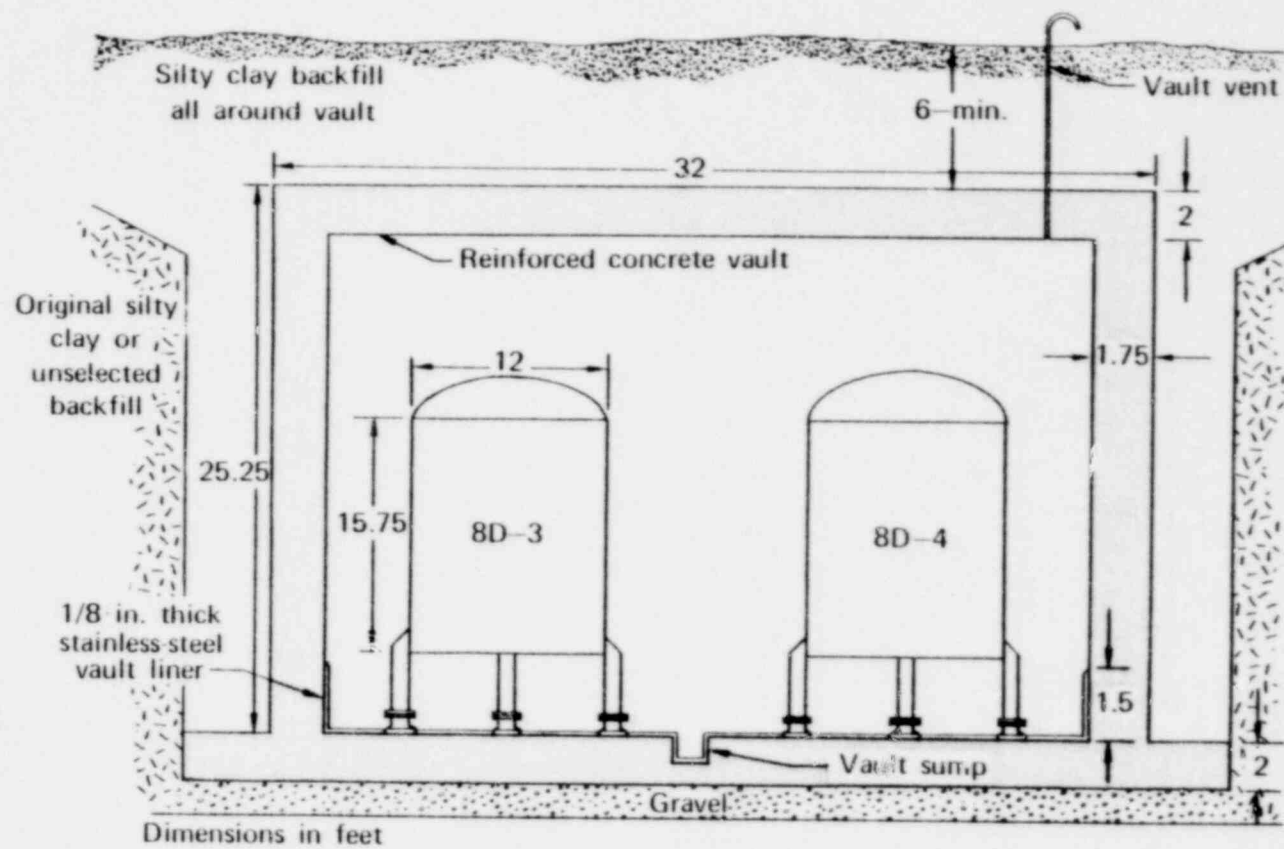


FIG. 2. Storage tanks 8D-3 and 8D-4, the reinforced concrete vault, and the liner.

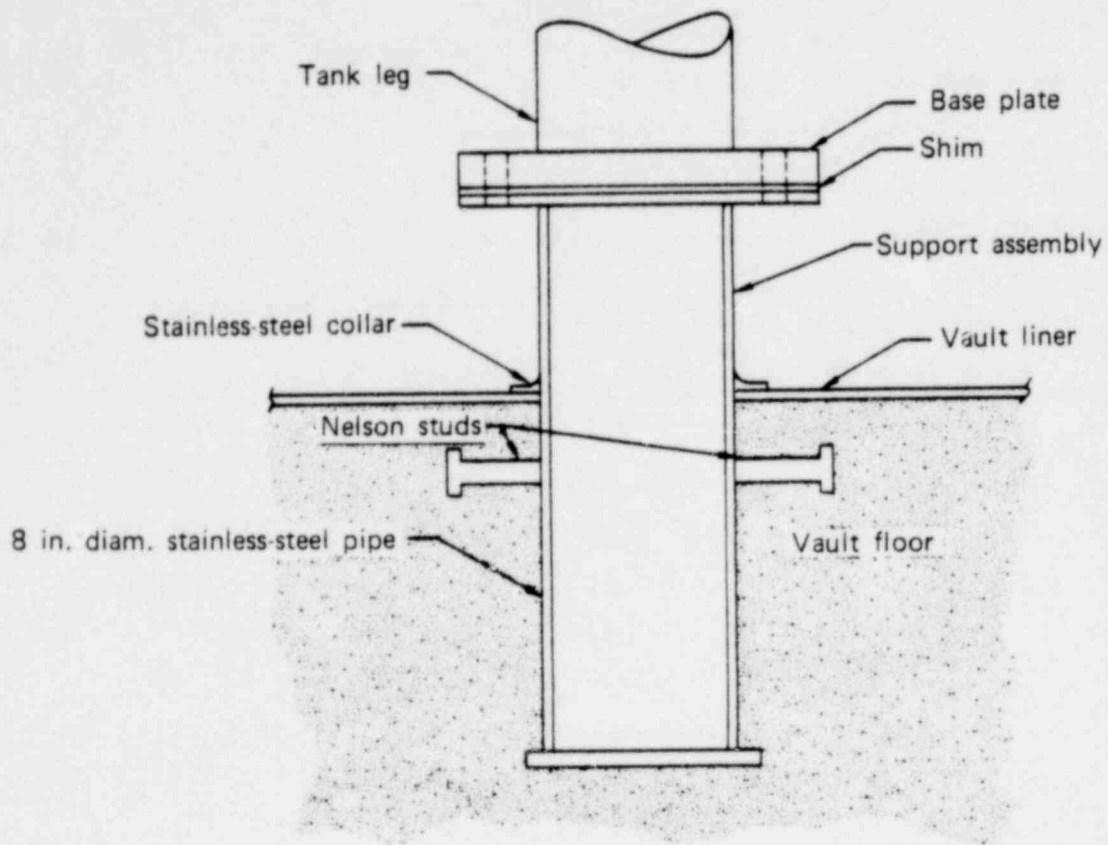


FIG. 3a. Close-up of tank leg support assembly.

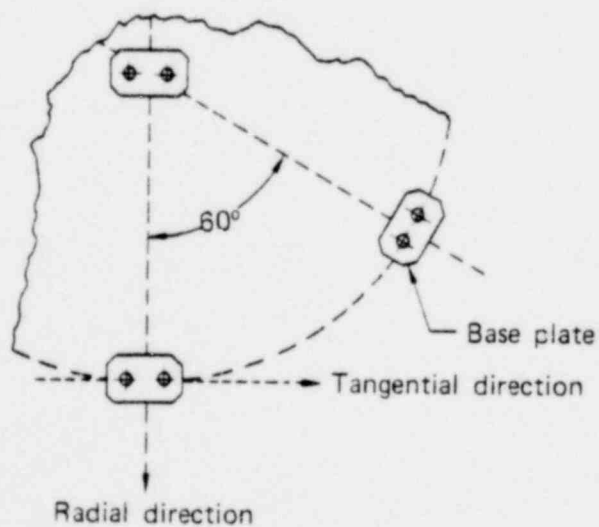


FIG. 3b. Plan view of base plate geometry.

MATHEMATICAL MODEL

The finite element technique was selected for modeling the waste storage tanks and the reinforced concrete vault because it can easily handle complex structures with different material properties, geometrical configurations, and boundary conditions. The computer program used is SAP4,⁵ the LLL version of a finite element computer program originally developed at the University of California at Berkeley.

We studied the arrangement and the connection between the tanks and the vault to determine if we needed one complete finite element model to describe both structural components. Because the waste storage tanks are fastened to the floor of the vault there is practically no feedback from the tanks to the vault. Therefore, separate mathematical models were developed for the tanks and the vault, and the analyses proceeded independently.

TANK ANALYSIS

There are two identical storage tanks, 8D-3 and 8D-4; however, only one now contains liquid waste. The tank with liquid waste in it is the critical one that will experience higher static and seismic loads and has to maintain its structural integrity during and after earthquakes. Therefore, the typical model for the tanks was selected to be the one with stored liquid waste.

TANK MODEL

Because of tank symmetry, only one quarter of the structure needed to be included in the mathematical model. Symmetrical boundary conditions were applied to the edges of the model for symmetrical loads such as dead weight and static liquid pressure. Anti-symmetrical boundary conditions were applied to the edges for such anti-symmetrical loads as seismic loading.

The shell of the tank was modeled by the quadrilateral plate/shell elements of SAP4. Stiffeners and support legs were modeled by beam elements. Cooling coils and guide brackets were not included in the model because they contribute no stiffness and negligible mass effects to the overall behavior of the structure.

Figure 4 gives a three-dimensional view of the finite element model, which consists of 90 plate/shell elements for the dome-shaped roof, the cylindrical shell wall, and the flat bottom plate. Also, there are 31 beam elements for the vertical legs and the radial and transverse stiffeners.

The support legs of the tanks, made of 8-in.-diam. extra strong pipe, are welded to a base plate, which is bolted to the support assembly by two bolts whose centers are aligned in the tangential direction (Fig. 3b). This alignment provides moment resistance about the radial direction but very little moment resistance about the tangential direction. This kind of boundary condition could be accurately modeled when the radial and tangential

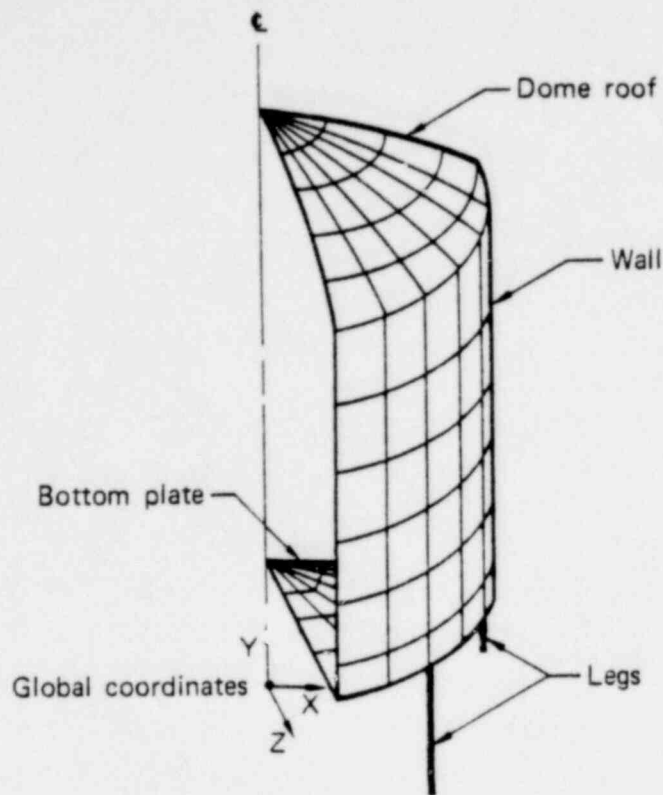


FIG. 4. Tank finite element model.

directions were parallel to the global directions of the finite element model. However, for the nonglobal direction supports, the boundary spring element of SAP4 had to be used to add a very large stiffness to constrain rotation about a radial line. This extra large stiffness did not cause problems in the static solution; however, it could create some numerical problem in the eigenvalue calculation. Hence, the nonglobal moment supports were fixed in both radial and tangential directions in the dynamic analyses. This is believed to have no significant influence on the final results.

The elastic modulus and Poisson's ratio for the steel are 29×10^6 psi and 0.3, respectively.

STRUCTURAL LOADING

Both static and dynamic loads were considered in the analysis of the tank.

Static Loads

Dead Load. The dead weight of the tank and its supporting members was included as a static load to the system. The density of steel used was 0.286 lb/in.³.

Hydrostatic Load. The hydrostatic pressure of the stored liquid waste was considered as a pressure load on shell elements. The level of liquid was assumed to be at the top of the shell wall (15.75 ft above the bottom plate). Hydrostatic pressure at the center of each shell element was taken to be the average pressure on it since each element can take only uniform pressure over it. The dead weight of the liquid was included in this case as pressure on the bottom plate.

Thermal Load. A cooling coil system keeps the solution temperature below 140°F. The thermal load due to the temperature gradient through the tank's thin wall is negligible. If the temperature during installation is assumed to be 70°F, the solution temperature of 140°F will have caused the tank to expand radially about 0.05 in., which is less than the tolerance of 3/32 in. for the base plate bolts. Therefore, the residual force due to thermal expansion is also negligible.

Seismic Loads

Ground excitations for the tank structure were based on the Safe Shutdown Earthquake (SSE) defined by NRC Regulatory Guide 1.60.⁶ We used two design response spectra from the guide--one for the horizontal component of ground motion and one for the vertical component (Fig. 5a and 5b). The curves are normalized to a peak ground acceleration of 1.0 g. For each analysis the curves can be scaled to appropriate maximum accelerations. Because the analyses are linear, scaling can be done on the input or the results. We found it more convenient to scale the results prior to combination of loads.

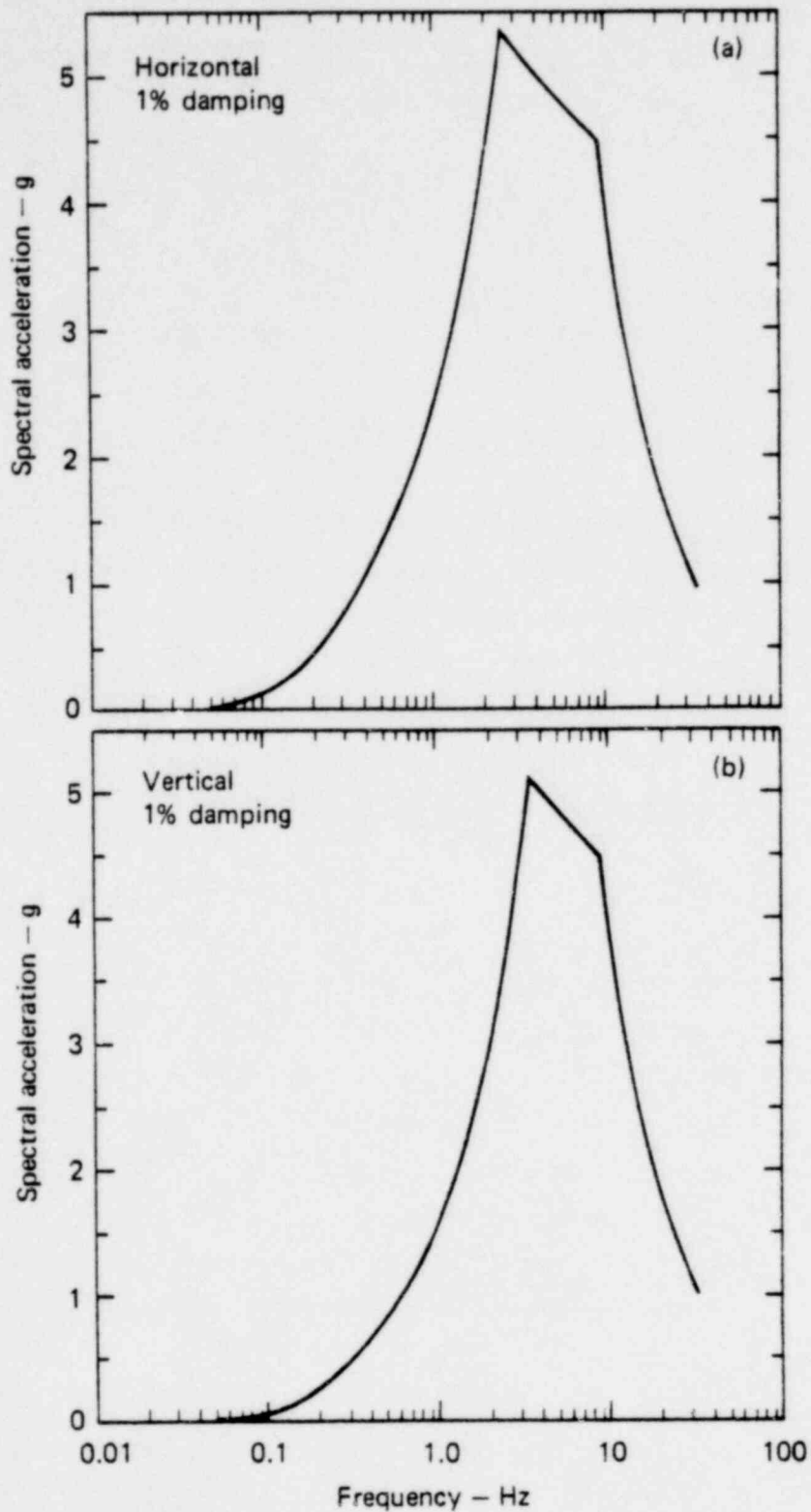


FIG. 5. Horizontal (a) and vertical (b) response spectra from NRC Regulatory Guide 1.60 normalized to 1.0-g peak ground acceleration.

505 5851

The seismic load was treated as a dynamic load on the structural system. Several seismically induced dynamic effects are discussed below.

Structural Inertia. SAP4 accounts for the inertia of the structural system as lumped masses at the structural nodes; that is, the distributed mass of an element is lumped to its nodes as concentrated masses. This assumption ignores the coupling inertia effect between different nodes and the rotational inertia of the distributed mass. However, the approximation is a good one for a reasonably refined finite element mesh.

Structural Damping. Damping of the structural system, which results from material, connections, etc., is assumed to be viscous in nature, hence, velocity dependent. Because damping, unlike stiffness and mass, is usually not clearly defined for a system, common practice is to assign damping ratios to the structural system based on experience. The damping ratio is defined as the ratio of the actual damping to the critical damping of the structure. According to Regulatory Guide 1.61,⁹ the damping ratio of welded steel structures subjected to a SSE is 4%. For structures containing fluid, however, the damping ratios are modified as discussed below.

Hydrodynamic Effect. The liquid stored in the tank will produce both impulsive and sloshing loads and will alter the critical damping of the system. The impulsive load is basically the inertia of the fluid, that is, the hydrodynamic pressure of the accelerated fluid on the structure. This pressure is proportional to the structural acceleration. Its magnitude and distribution can be obtained by solving the governing Laplace equation with the given boundary conditions. The following expression provides estimates of the pressure distribution on the inside wall of a rigid cylinder subjected to a small impulsive excitation, a .¹⁰

$$P = -\gamma a \cos \theta \frac{16H}{\pi^2} \sum_{n=1,3,5}^{\infty} \frac{(-1)^{(n-1)/2}}{n^2} \cos \frac{n\pi Z}{2H} \frac{I_1\left(\frac{n\pi R}{2H}\right)}{I_0\left(\frac{n\pi R}{2H}\right) + I_2\left(\frac{n\pi R}{2H}\right)},$$

where

- H = the liquid depth
- R = the inside radius of the cylinder
- r, θ, Z = the cylindrical coordinates
- γ = the mass density of the liquid
- $I_0, I_1,$ and I_2 = the modified Bessel functions of orders 0, 1, and 2.

To include this effect, P/a can be treated as an additional mass to the structure. The amplitudes (at $\theta = 0$) of this added mass distribution for tanks with different R/H ratios are shown in Fig. 6 ($R/H = 0.38$ in this study). Because SAP4 cannot take distributed added mass, the distributed mass was first lumped to the proper nodal points, and the lumped masses were input as concentrated masses.

The sloshing load is due to surface waves of the accelerated fluid. Sloshing pressure is small relative to the impulsive pressure for this type of tank.¹¹ Our conservative assumptions about liquid level, rigid tank, etc., justify neglecting sloshing forces in this analysis.

Drag and other damping forces in the fluid are difficult to adequately include in the analysis. For tanks with large radii, such as this tank, the damping effect of the fluid is usually negligible. The only damping force in the fluid-structure system is, therefore, assumed to come from the structural damping. However, the critical damping of the system changes because of the increased total mass.¹² Consequently, the damping ratio of the fluid-included system has to be changed according to the following expression:

$$\zeta_{\text{fluid}} = \sqrt{\frac{M}{M}}$$

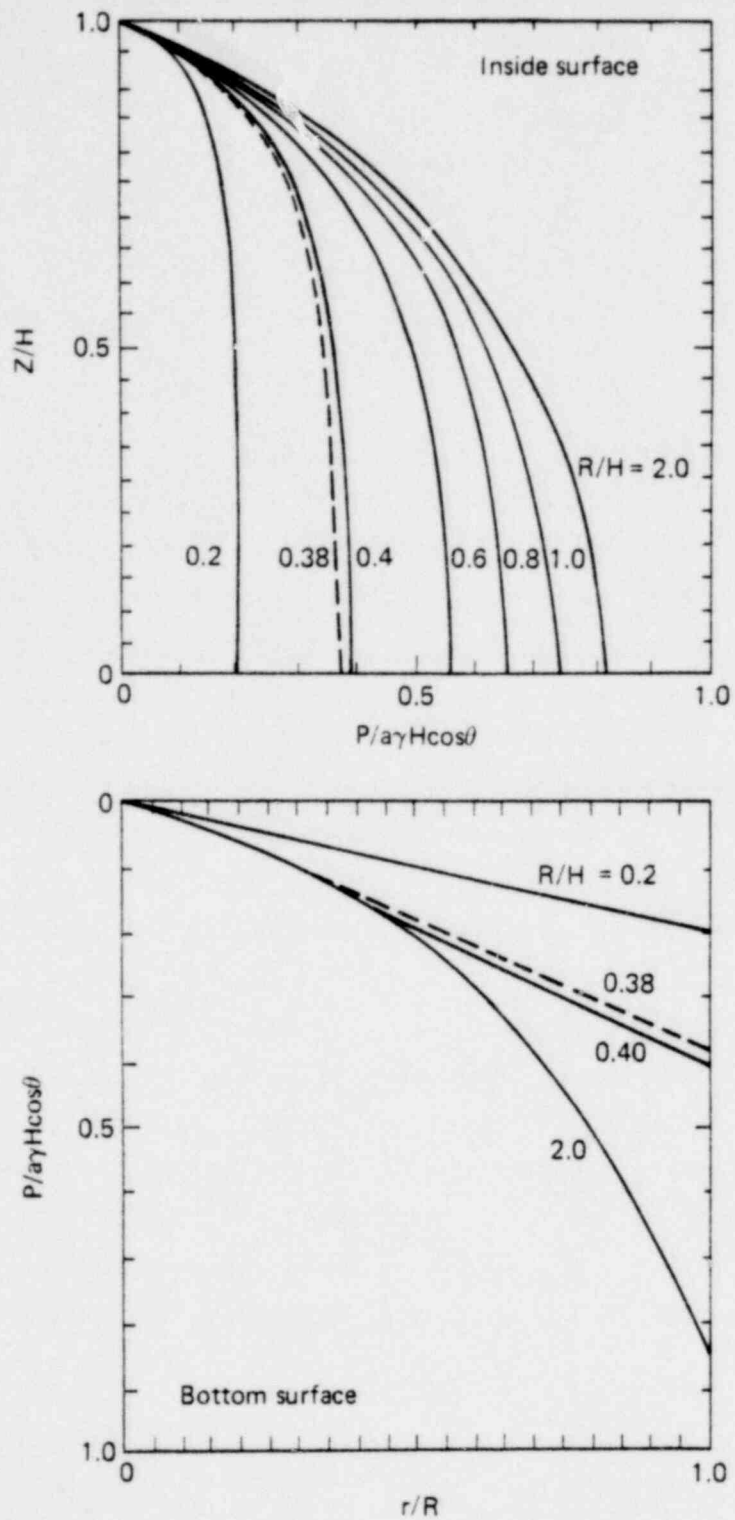


FIG. 6. Hydrodynamic pressure, P , resulting from a small impulsive excitation, a , on the inside wall of a rigid cylinder is accounted for as an added mass P/a . (Other symbols are identified in the text.)

where ξ and M are the damping ratio and the mass, respectively, of the structure alone. $\bar{\xi}$ and \bar{M} are the damping ratio and the mass, respectively, of the fluid-structure system.

For this tank, $M = 35.33 \text{ lb-sec}^2/\text{in.}$, $\bar{M} = 421.08 \text{ lb-sec}^2/\text{in.}$ and $\xi = 0.04$. Therefore, $\bar{\xi} = 0.01$ and the damping ratio of 1% was used for all modes of the structural system.

SEISMIC ANALYSIS METHOD

Seismic responses of the tank were computed by the response-spectrum technique in which the natural frequencies and mode shapes of the structural system are found by an eigenvalue/eigenvector analysis of the mathematical system. Usually in earthquake analyses, linear combinations of several mode shapes with the lowest frequencies are sufficient to represent all different deformations of the structure. Peak responses of each mode are obtained but relative phasing information is not. Consequently, we can calculate directly the maximum responses of each mode from the spectrum curve but not the true maximum response of the structure. Our estimates of maximum response were obtained by taking the square root of the sum-of-the-squares (SRSS) of the modal components.

COMBINATION OF LOADS

Peak responses for the input earthquake result from either the response-spectrum analysis used for the tank or the equivalent static analysis used for the vault. Because the three components (two horizontal and one vertical) of the input earthquake are treated separately, each component has its corresponding peak response, and the three peak responses usually do not occur at the same time. One common way to calculate the combined peak response is to take the SRSS of the three peak responses. This approach assumes that the peak responses occur at statistically independent times. This is a reasonable assumption for structures with well-separated natural frequencies. In this

1185 SPT

case, the peak accelerations of the three input earthquake components were given the ratios of 1 (horizontal) to 1 (horizontal) to 2/3 (vertical).

A way of combining components that was recommended by Newmark¹³ was also used. The combined peak response is the direct sum of responses to input motions having peak accelerations in the ratios of 1.0 (horizontal) to 0.4 (horizontal) to 0.4 (vertical).

The combined responses of static loads and seismic loads are the sums of responses to these two types of loads. However, the seismic responses obtained from either the response-spectrum method or the equivalent static method are the absolute values of the peak responses; hence, they can be either positive or negative peaks. Therefore, separate results were obtained for cases of the static responses added to the positive seismic responses as well as to the negative seismic responses.

LIMITING CRITERIA

An accurate definition of limiting criteria for either the thin shell tank structure or the reinforced concrete vault structure are difficult to obtain because of the complex nature of the loading and the nonlinear behaviors of the structural members and surrounding soil medium. The set of limiting criteria that we established for each structural component represents a reasonably conservative estimate of the start of structural distress.

Stress results of the tank were studied for the following three critical cases:

- Yielding or buckling of the shell wall
- Yielding of the bottom plate
- Yielding or buckling of the support legs and stiffeners.

A simplified formula for determining the critical buckling stress of a cylindrical shell under uniaxial compression is:

$$\sigma_{cr} = f \frac{Eh/a}{[3(1-\nu^2)]^{1/2}}$$

where

h = shell thickness

a = radius

E = elastic modulus

ν = Poisson's ratio, and

f = reduction factor depending on the a/h ratio.

For this tank $a/h = 230.4$, $f = 0.23$ (Ref. 3, p. 38), $E = 29 \times 10^6$ psi and $\nu = 0.3$. Therefore, $\sigma_{cr} = 17.5$ ksi. This critical buckling load does not consider the internal pressure from the liquid, which would make the critical buckling stress even higher. However, this formula gives a conservative value. Calculated axial compressive stresses for each element of the shell were checked against this limiting criterion of $\sigma_{cr} = 17.5$ ksi.

Limiting behavior of the tank (shell wall and bottom plate) was based on the criterion that the Von Mises stresses exceeded the 25-ksi yielding stress of the material (A240-TP304L). At each stress location, two Von Mises stresses were calculated, one associated with the outside surface of the tank, and the other associated with the inside surface of the tank. To determine the Von Mises stress at a location having static stress components σ_{xs} , σ_{ys} , and τ_{xys} and dynamic stress components σ_{xd} , σ_{yd} , and τ_{xyd} , we first calculated six combined stresses,

$$\begin{aligned}\sigma_x &= \sigma_{xs} \pm \sigma_{xd} \\ \sigma_y &= \sigma_{ys} \pm \sigma_{yd} \\ \tau_{xy} &= \tau_{xys} \pm \tau_{xyd}.\end{aligned}$$

The plus and minus signs are used because the dynamic stress components can be either positive or negative. These six stresses give rise to eight different possible Von Mises stresses calculated by the formula:

$$\sigma_{VM} = \left(\sigma_x^2 - \sigma_x \sigma_y + \sigma_y^2 + 3\tau_{xy}^2 \right)^{1/2} .$$

The maximum of these eight values was taken as the Von Mises stress at that location, and compared to the yield stress to determine if the limit had been exceeded.

The limiting capacities of the support legs, stiffeners, and base plates were determined by comparing the maximum stresses in each member with the yield stress of the material.

RESULTS

Four separate analyses were conducted for the tank model:

- A static analysis using all static operating loads including dead load and hydrostatic pressure.
- Two response-spectrum analyses using the horizontal Reg. Guide 1.60 design response spectrum applied in two perpendicular directions (X and Z directions in the mathematical model).
- A response spectrum analysis using the vertical design response spectrum.

Before these four basic cases were analyzed, we determined the number of modes required to describe the dynamic behavior of the tank. The same horizontal spectrum was used in models having 5, 10, and 15 modes. The highest frequencies for these three models were 12.4, 18.7, and 29.1 Hz respectively. Force and stress results differed by less than 1% between the 5- and 10-mode systems, and there was no practical difference between the 10- and 15-mode systems. We concluded that ten modes were sufficient for the response spectrum analyses.

Peak ground accelerations for both the horizontal and vertical spectra were scaled to 0.2 g. As discussed previously, ground motion components were combined in two ways. The first one used the same peak ground acceleration level in both horizontal directions and 2/3 the level in the vertical direction. The responses to these three components were then combined by the SRSS method and added to the static results. The second method used 100% in

the major horizontal direction and 40% in both the minor horizontal and vertical directions, and the responses were added directly to the static responses.

The eight Von Mises stresses on each face of each element were calculated for both combination methods. The corresponding peak accelerations at which the Von Mises stress reached the yield stress were then computed.

The combined stress results, calculated by either the SRSS method or the direct sum method, show that the stresses in the tank wall at peak acceleration of 0.2 g are lower than our limiting criteria. Results computed by those two combination methods differ insignificantly. Neither method gives consistently high values. As expected, the highest Von Mises stress occurred in the area of the tank wall near the legs. The value computed was 40% of the yield stress by the direct sum method and 39% by the SRSS method.

The legs have a maximum stress of 18 ksi. The highest stress in the bottom plate stiffeners is about 50% of the yield stress.

The highest stressed members in the tank structure are the base plates that connect the legs to the support assembly. The bending stress in the plates is 31 ksi at 0.2 g, while the yield stress is 25 ksi. This will cause part of the base plate to yield but will not affect the supporting function of the leg.

VAULT ANALYSIS

VAULT MODEL

The vault is basically a reinforced concrete rectangular box buried 6 ft underground. A three-dimensional finite element analysis, including nonlinear soil-structure interaction, is beyond the scope of this study. However, an equivalent static analysis, which includes the dynamic effects of the surrounding soil by applying the peak dynamic soil pressure on the structure, is considered to be both adequate and conservative. Therefore, only the structure itself needs to be included in the model.

Two types of elements are available in SAP4 to model the reinforced concrete wall of the vault. One is the plate/shell element used for the tank model. The other is the three-dimensional solid element, which behaves better through the thickness than do plate/shell elements. However, this type of element provides stress results only at a few selected stress points, unlike plate/shell elements, which give moments and forces on the section. To evaluate the resisting capacity of the reinforced concrete section, the moment and force results of a plate/shell element are more convenient and straightforward to use. The effect of through-the-thickness variation is expected to be minimum. Therefore, the walls and roof of the vault were modeled by plate/shell elements.

In modeling the stiffness of the vault, the reinforced concrete walls and roof were assumed to be homogenous and isotropic. However, in estimating the limiting capacities of the structure, cracked concrete sections were considered. The elastic modulus and Poisson's ratio for the concrete are 3×10^6 psi and 0.17, respectively.

The walls were assumed to be fixed at the base. The floor was assumed to be rigid and not included in the model. The six horizontal girders (W 12 x 27) in the roof were modeled by beam elements.

An auxiliary shelter on top of the roof was also modeled by plate/shell elements; however, the cover of the shelter was not included.

Only half of the structure was included in the mathematical model because of the vault's symmetry. Figure 7 shows the three-dimensional view of the finite element model, which has 118 plate/shell elements and 31 beam elements.

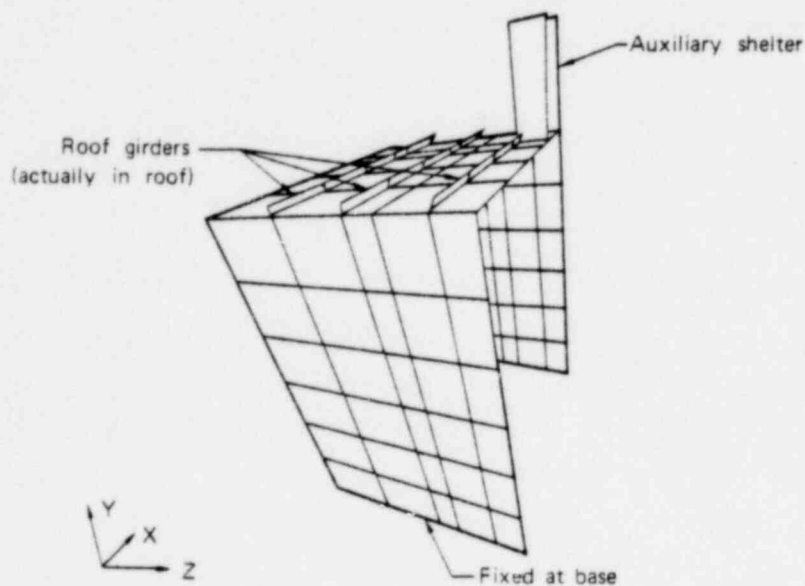


FIG. 7. Finite element model of vault.

STRUCTURAL LOADING

Dead load, static soil pressure, thermal load, and seismic load were considered in the analysis of the vault.

Static Load

Dead Load. The weights of the walls and the roof of the vault were included as part of the static load. The density of the reinforced concrete was taken to be 150 lb/ft^3 .

Static Soil Pressure. The weight of 6 ft of soil on top of the roof was included as a static pressure, which was calculated by the following formula:

1792 271

$$P = \gamma h ,$$

where

γ = soil density, 130 lb/ft³

h = soil depth.

The lateral pressure on the side walls was calculated as

$$P = K_A \gamma h$$

where K_A is the lateral force coefficient. A value of 0.3 was used in this study.¹⁴

Thermal Load. Because the stored waste temperature is about 140°F, we assumed that the temperature on the inside surface of the concrete vault is about 140°F. The outside surface of the vault and the surrounding soil will remain at a lower temperature. The temperature difference through the vault wall can cause significant thermal stresses in the structure. Evaluation of thermal forces in reinforced concrete members is a complicated problem. Cracking of the section, creeping of the concrete, and the self-releasing nature of thermal forces make the phenomenon nonlinear. The problem is more difficult in this study because we do not have an accurate measure of the actual temperature on either surface of the vault. A conservative estimate of the temperature gradient was 70°F. The analysis was conducted with this value and with the assumption that the structure remained linear. The coefficient of thermal expansion used for concrete was $7 \times 10^{-6}/^{\circ}\text{F}$.

Seismic Load

A complete dynamic analysis of the embedded structure requiring a nonlinear time history analysis of the finite element system including the surrounding soil and the vault is beyond the scope of this study. A simpler approach is to treat the dynamic loads, including the inertial load of the structure and the dynamic soil pressure, as equivalent static loads. The applied equivalent static load is the estimated peak dynamic load. This approach, which neglects the dynamic amplification and damping effects of the structural system, usually gives good results for stiff structures.

Equivalent static responses to the inertial loads of the structure were obtained by applying peak ground accelerations as gravity loads in the three corresponding finite element global directions.

It is difficult to find the equivalent static load that can truly represent the dynamic effects of the surrounding soil. Mononobe⁷ and Okabe⁸ developed a method for determining the maximum dynamic lateral pressure on a retaining structure. A detailed discussion of this method was given by Seed and Whitman.¹⁴ This method basically assumes that the dynamic pressure has the same distribution as the static soil pressure with a modification factor to account for dynamic behavior of the soil and the retaining structure. Further studies¹⁵ indicate that the dynamic soil pressure distribution differs from the static pressure distribution. However, not much information is available regarding the dynamic soil pressure on embedded structures. A previous study³ using a finite element model of an embedded vault showed that a conservative estimate of the peak dynamic soil pressure is given by the equivalent static pressure, P , as follows:

$$P = \frac{3}{4} \frac{A_H}{g} \gamma H \left(1 - \frac{h}{H}\right) K ,$$

where

γ = soil density

h = soil depth

A_H = the peak horizontal ground acceleration

H = soil depth at the bottom of the structure

K = a correction factor based on finite element model study.

The pressure distribution from this expression is an inverted triangle with maximum pressure at the top of the structure and zero pressure at the bottom.

Applying this pressure distribution to the vault model raises the problem of whether negative pressure (tension) should be applied on the far wall when positive pressure is applied to a near wall. The surface between the silty clay backfill and the concrete wall cannot develop significant tensile forces. However, because the walls are always subjected to static soil compression, the negative dynamic soil pressure should be able to release a portion of the static pressure.

ATS 5001

Figure 8a shows the vault in cross section and gives the bending moments for the case of positive pressure acting on one wall. Figure 8b shows the bending moments for the case of negative pressure acting on the opposite wall. In both cases, pressure on a wall induces insignificant bending moments in the opposite wall.

Figure 8c shows the combined case of positive pressure on one wall and negative pressure on the opposite wall. We are interested only in the absolute value of the total response. Although only a portion of the negative pressure may develop, we have included the complete negative pressure on the far side of the vault to be conservative.

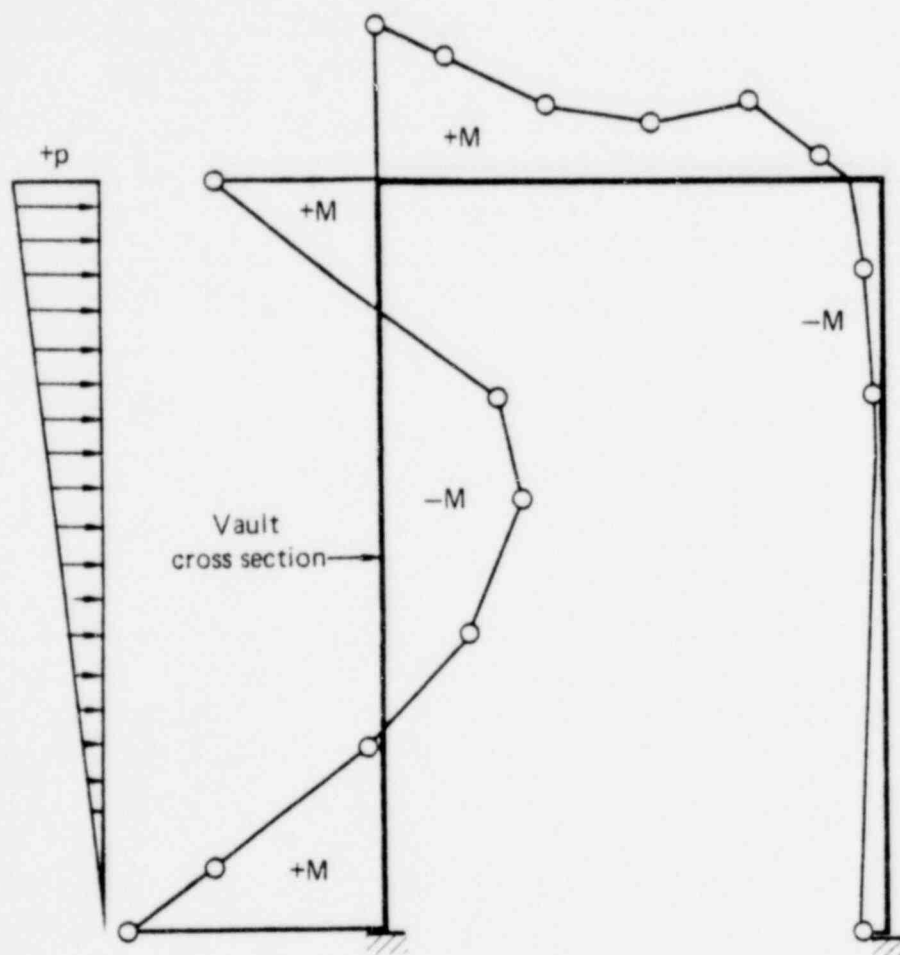


FIG. 8a. Bending moments, M , that result from positive pressure acting on the left side of the vault (shown in cross section).

1792 274

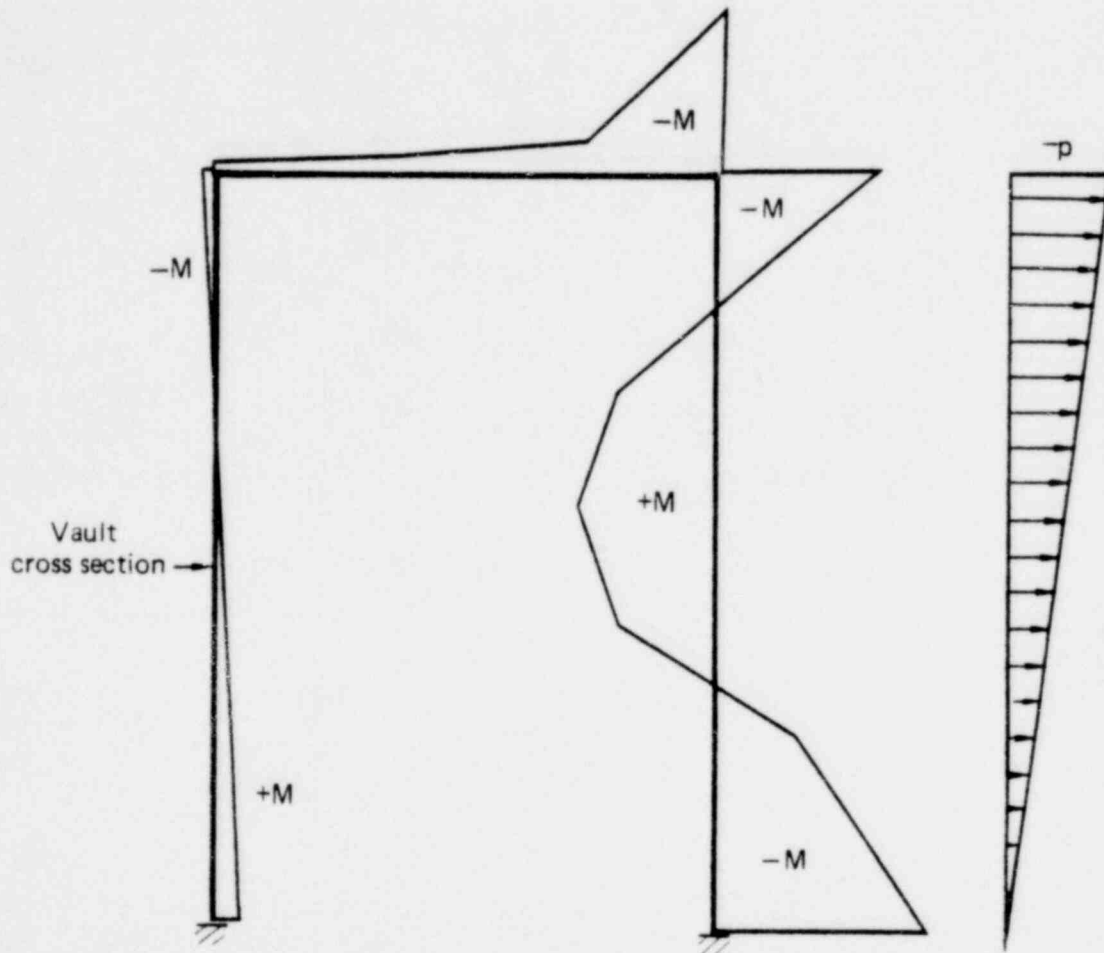


FIG. 8b. Bending moments that result from negative pressure acting on the right side of the vault (Note: Pressure on one side of the vault produces insignificant bending in the opposite wall).

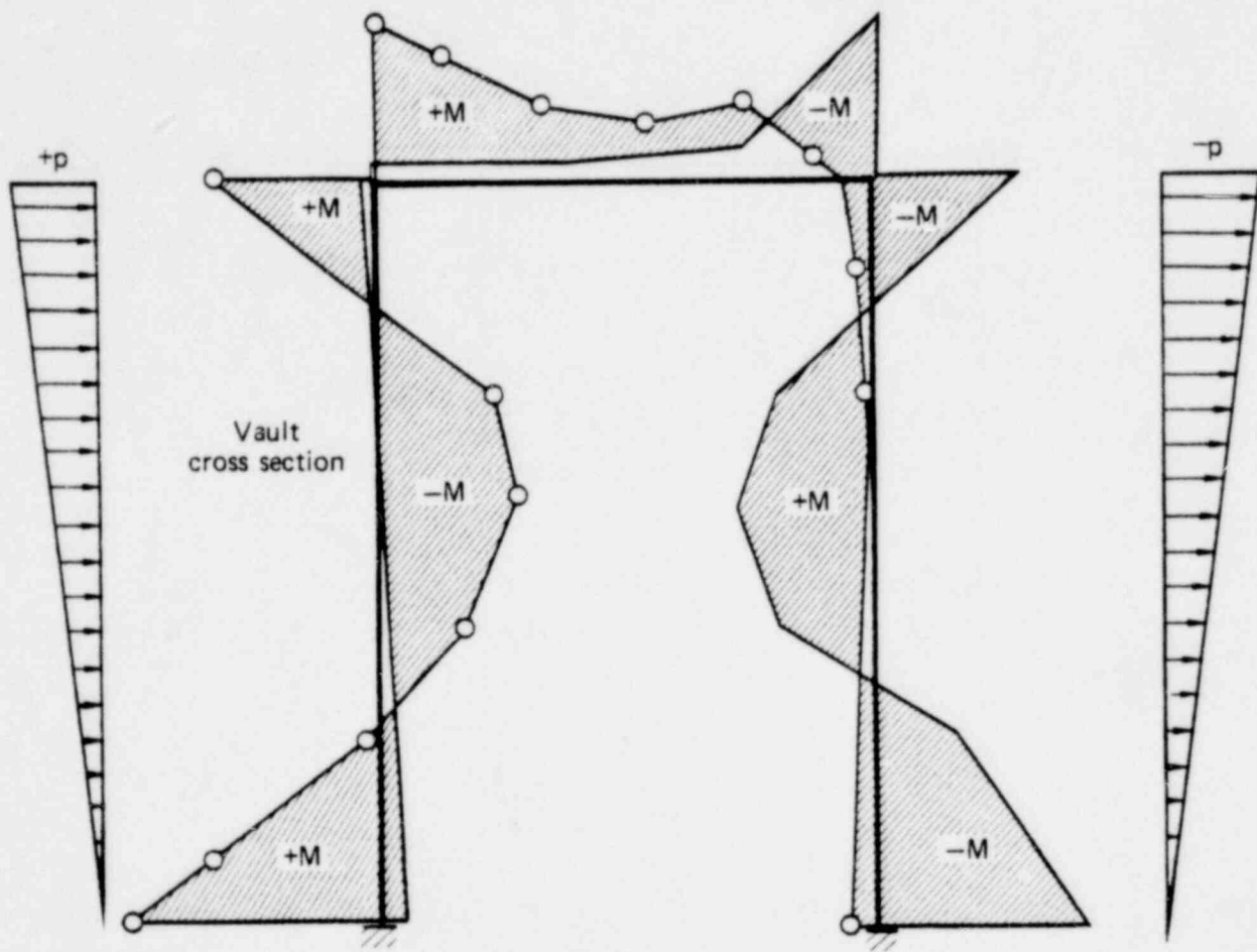


FIG. 8c. Combined bending moments resulting from positive pressure on one side of the vault and negative pressure on the other side.

SEISMIC ANALYSIS METHOD

An equivalent static method was used for the seismic analysis of the vault. The dynamic amplification effect of the structure is not explicitly included in this method. The inertial effect of the vault was included by applying a uniform static load of the peak ground acceleration in the direction of excitation. The dynamic soil pressure was represented by the equivalent static pressure as discussed previously. It is reasonable to assume that the equivalent static approach can give a good estimate of the peak dynamic response of the system for the following reasons: the predominant dynamic force for the vault is the dynamic soil pressure, and the dynamic behavior of the soil-structure system has already been considered in deriving the equivalent static pressure.

COMBINATION OF LOADS

The two dynamic effects--the inertia of the structure and the dynamic pressure of the surrounding soil--were analyzed separately in the equivalent static analysis of seismic load for the vault model. For each earthquake component, these two responses must be combined to give the response to that component. The inertial response and the dynamic soil pressure response were combined by the SRSS method because the two responses are not in phase.

LIMITING CRITERIA

The major structural members of the vault are the reinforced concrete walls and roof. The walls and the roof were modeled by plate/shell elements, and the stress results were given in two perpendicular in-plane directions in the form of in-plane stresses and moments. Limiting conditions were defined by the following two equations for each element.

$$F_x = \left| \frac{S_{xx}}{S_{xxu}} \right| + \left| \frac{S_{xy}}{S_{xyu}} \right| + \left| \frac{M_{xx}}{M_{xxu}} \right| + \left| \frac{M_{xy}}{M_{xyu}} \right| \leq 1 \quad (1)$$

and

$$F_y = \left| \frac{S_{yy}}{S_{yyu}} \right| + \left| \frac{S_{xy}}{S_{xyu}} \right| + \left| \frac{M_{yy}}{M_{yyu}} \right| + \left| \frac{M_{xy}}{M_{xyu}} \right| \leq 1 \quad (2)$$

The terms, S_{xx} , S_{yy} , S_{xy} , M_{xx} , M_{yy} , are the resultants in the local x and y directions of stresses and moments (per unit length). Two cases were studied in defining the total resultant forces, which were defined as the static forces plus or minus the absolute values of the dynamic forces, i.e.,

$$S_{xx} = (S_{xx})_S \pm \left| (S_{xx})_D \right|, \text{ etc.}$$

The terms, S_{xxu} , S_{yyu} , S_{xyu} , M_{xxu} , M_{yyu} , and M_{xyu} are the calculated element limiting capacities for the reinforced concrete section. They are defined as follows:

$$S_{xxu} \text{ (or } S_{yyu}) = A_s f_y / A_g, \text{ if } S_{xx} > 0 \text{ (or } S_{yy} > 0) \text{ (Tension)}$$

$$S_{xxu} \text{ (or } S_{yyu}) = 0.85 f'_c + A_s f_y / A_g, \text{ if } S_{xx} < 0 \text{ (or } S_{yy} < 0) \text{ (Compression)}$$

$$S_{xyu} = 2 \sqrt{f'_c} + A_s f_y / A_g \text{ (Shear)}$$

$$M_{xxu} \text{ (or } M_{yyu}) = A_s f_y (d-a/2) \text{ (Bending)}$$

$$M_{xyu} = 2 \sqrt{f'_c} A_g t \text{ (Torsion)}$$

where

A_s is the area of reinforcing steel per unit length of the wall or roof in x or y direction

A_g is the gross area per unit length of the wall or roof in the x or y direction

f_y is the yield stress of the steel (60,000 psi in this case)

f'_c is the 28-day compressive strength of the concrete

$(f'_c = 5,000 \text{ psi for the wall and } 3,750 \text{ psi for the roof})$
 d is the effective depth of the reinforced concrete section
 $a = A_s f_y / 0.85 f'_c$
 t is the thickness of the section.

The limiting capacities of steel roof girders were determined by comparing the maximum stress in the member with the yield stress of the material.

RESULTS

The equivalent static analysis method was used to analyze the seismic dynamic loads on the vault. The seven basic static analyses are shown in Table 2.

TABLE 2. Seven basic static analyses of vault and scaling factors used to account for different peak accelerations of the three input earthquake components.

Case no.	Load	Scaling factor	
		SRSS method	Direct sum method
(1)	Dead load plus static soil pressure	1	1
(2)	Inertial load, 0.2 g, in the horizontal X direction	1	1
(3)	Inertial load, 0.2 g, in the vertical Y direction	2/3	0.4
(4)	Inertial load, 0.2 g, in the horizontal Z direction	1	0.4
(5)	Dynamic soil pressure in X direction for 0.2 g acceleration	1	1
(6)	Dynamic soil pressure in Z direction for 0.2 g acceleration	1	1
(7)	Thermal gradient of 70°F through the thickness	1	1

Results were scaled prior to combination of loads to reflect the different peak accelerations of the three input earthquake components. The scaling factors were 2/3 for case 3 for the SRSS method and 0.4 for cases 3 and 4 for the direct sum method. The SRSS method required a direct sum of case 1 and 7 then added to it the SRSS value of the other five cases (Fig. 9). The direct sum method required the sum of cases 1, 3, 7, the SRSS value of cases 2 and 5 and the SRSS value of cases 4 and 6.

Comparisons were first made between results computed by the two different methods of combination. The limiting condition factors F_x and F_y , defined by Equations 1 and 2, differ by less than 10% when results from the two methods are compared. For most elements, the SRSS method gives high values because it uses larger vertical and minor horizontal components of ground motion (0.13 g and 0.2 g vs 0.08 g and 0.08 g). The vault may be more sensitive than the tank to those two secondary components of the ground motion because of its large roof mass. The more conservative results calculated by the SRSS method are presented.

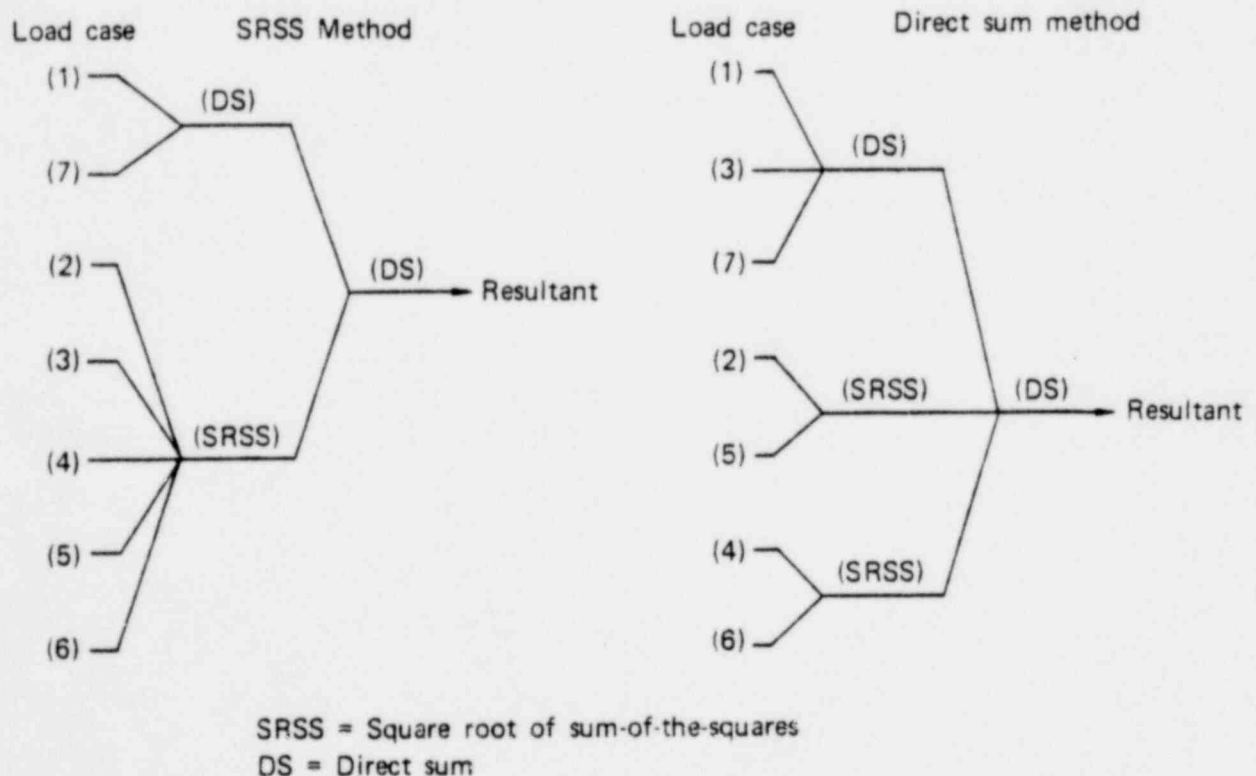


FIG. 9. Methods used to combine the seven basic static analyses in Table 2.

The structural responses obtained for the concrete vault confirmed an observation discussed in two previous studies of the NFS facilities, mainly, that bending moments induced by the thermal gradient of 70°F in the walls and roof far exceeded the ultimate moment capacities of the concrete section. The fact that the vault still exists and shows insignificant structural damage indicates that the thermal stress was overestimated in the analyses. Several possible explanations for the discrepancy are discussed below:

- The gradient of 70°F may be too high. Because the inside surface temperature of the vault built up over a long period of time, the outside surface of the wall and the surrounding soil had enough time to respond. The actual outside surface temperature may be higher than assumed; thus, the gradient may be smaller than 70°F.
- Thermal loads can be self-relieving because of creep and formation of cracks in the concrete. Thermal loads are related to the stiffness of the structure. As cracks and creep develop in the concrete, both stiffness and thermal load are reduced.

Although we believe that the thermal loads are lower than those predicted on the basis of a 70°F gradient, we do not know if the thermal loads should be ignored completely or partially included.

To account for cracking of the concrete, a reduction factor for the thermal stress of 0.3 to 0.4¹⁶ has been suggested for use when bending is prevalent, which will be the case for the vault if the thermal load is the predominant load. A factor higher than 0.4 should be used if the thermal gradient is small and not many cracks develop. In general, a large thermal gradient will cause high elastic stresses and many cracks, hence, a low reduction factor (high reduction). On the other hand, a small thermal gradient will give low elastic stress and few cracks, hence, a high reduction factor (low reduction).

Because we do not adequately know the thermal stress in the vault, the combined static, thermal, and dynamic results for the vault are presented in five different cases with 0, 25, 50, 75, and 100% of the thermal load for

$\Delta T = 70^{\circ}\text{F}$. The results can be interpreted as cases with thermal gradients of 0° , 17.5° , 35° , 42.5° , and 70°F and no reduction factor, or as cases having higher ΔT and reduction factors.

If there is no thermal gradient, limiting criteria are not exceeded with peak ground acceleration up to 0.2 g. Figures 10 to 13 show the regions where limiting criteria are exceeded and give the associated peak ground accelerations for the other four cases.

With a 25% thermal load (Fig. 10) limiting criteria are exceeded at only a few places near the center of the structure at 0.2-g acceleration.

For the 50% thermal load (Fig. 11) a small area of the edges of the roof near the center of the vault exceed the criteria at peak accelerations below 0.04 g. More extensive areas are affected at end walls when the peak acceleration reaches 0.12 to 0.16 g.

If the thermal load is 75% of the maximum (Fig. 12), the roof of the vault and much of the walls will exceed the limiting criteria at 0.02-g peak ground acceleration. With the full thermal load, (Fig. 13) almost the entire vault exceeds our limiting criteria.

The maximum stress in roof girders is less than the yield stress of the steel even for the full thermal load and 0.2-g peak acceleration.

185 5911

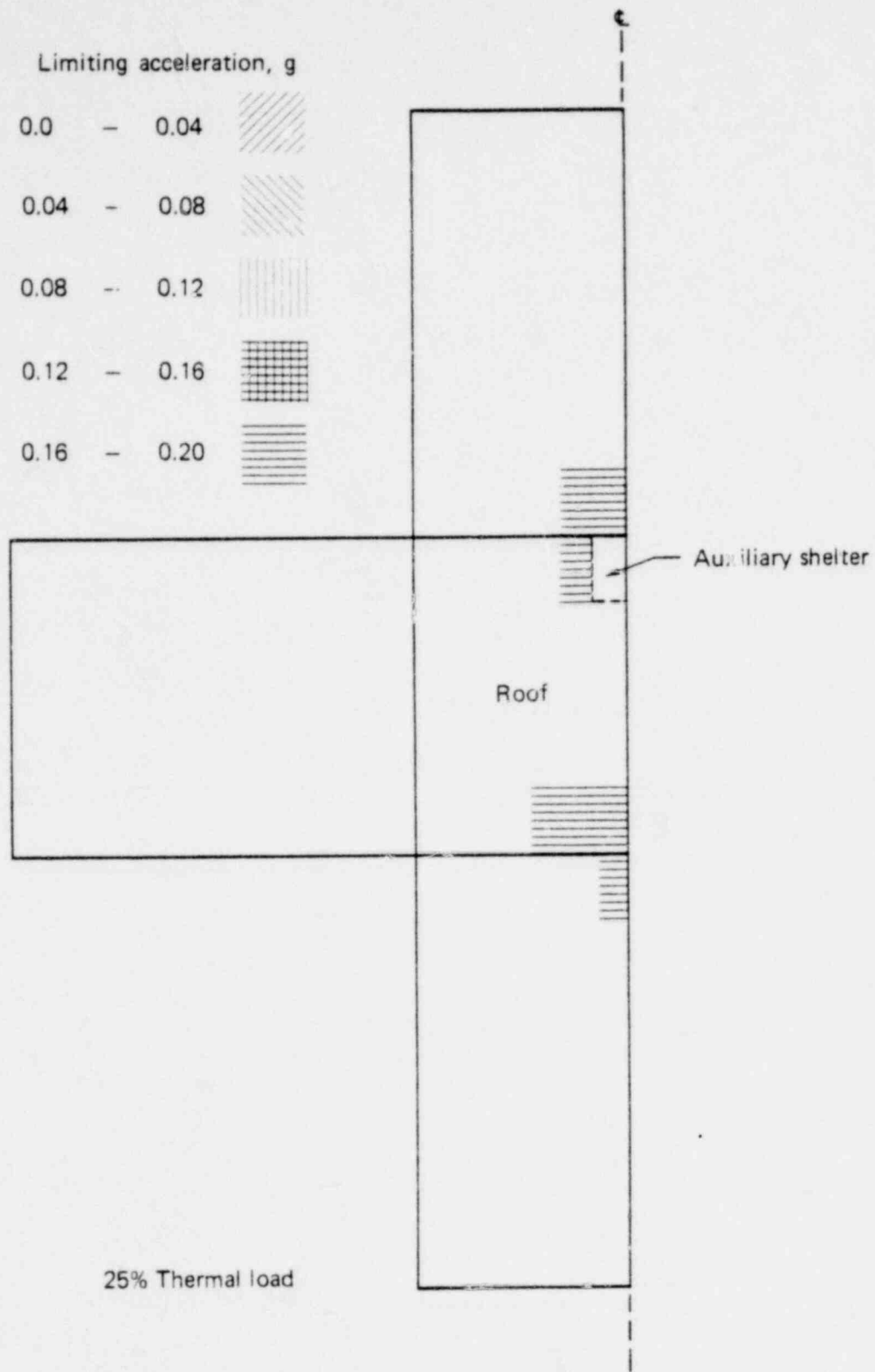


FIG. 10. Regions of vault model where limiting criteria are exceeded with 25% of the base thermal load included in the analysis.

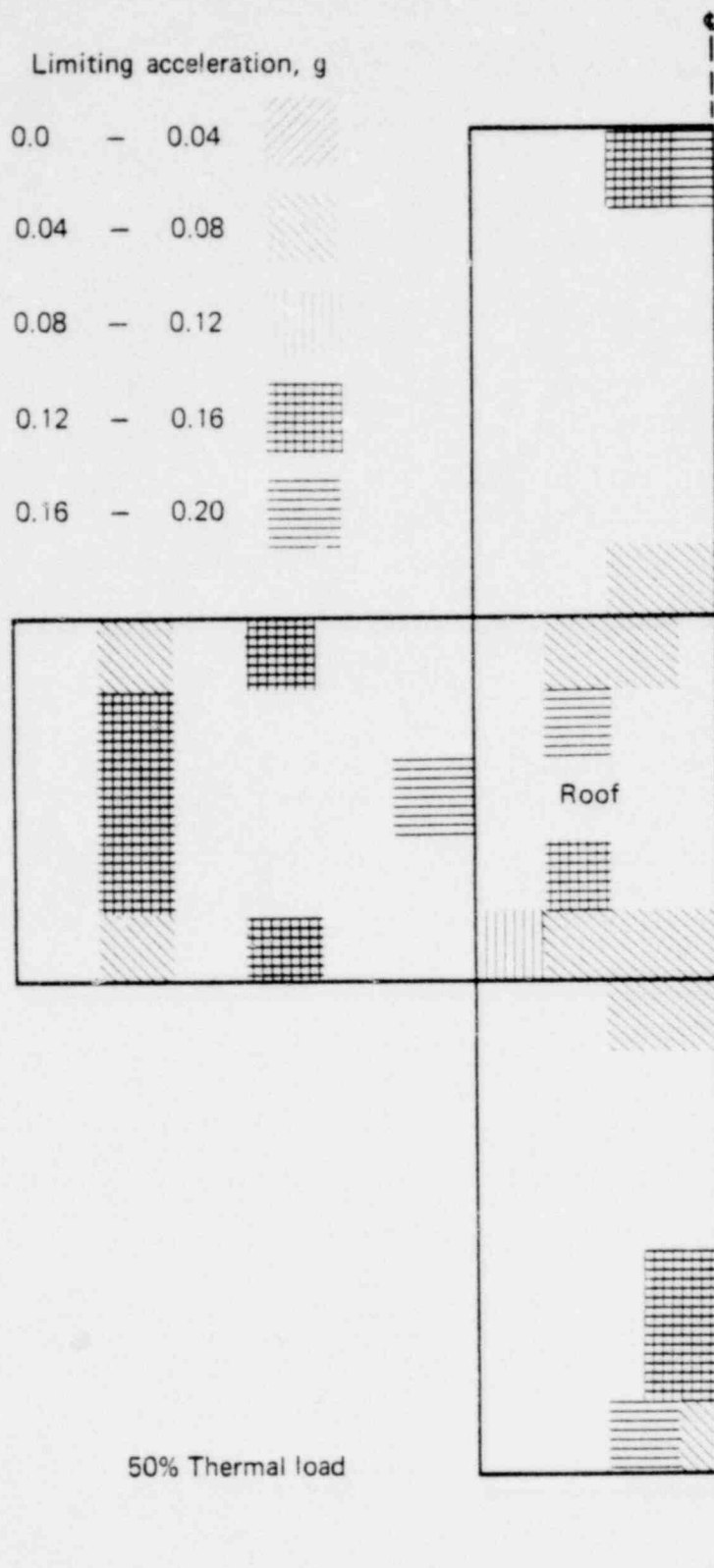


FIG. 11. Regions of vault model where limiting criteria are exceeded with 50% of the base thermal load included in the analysis.

885 SPV1

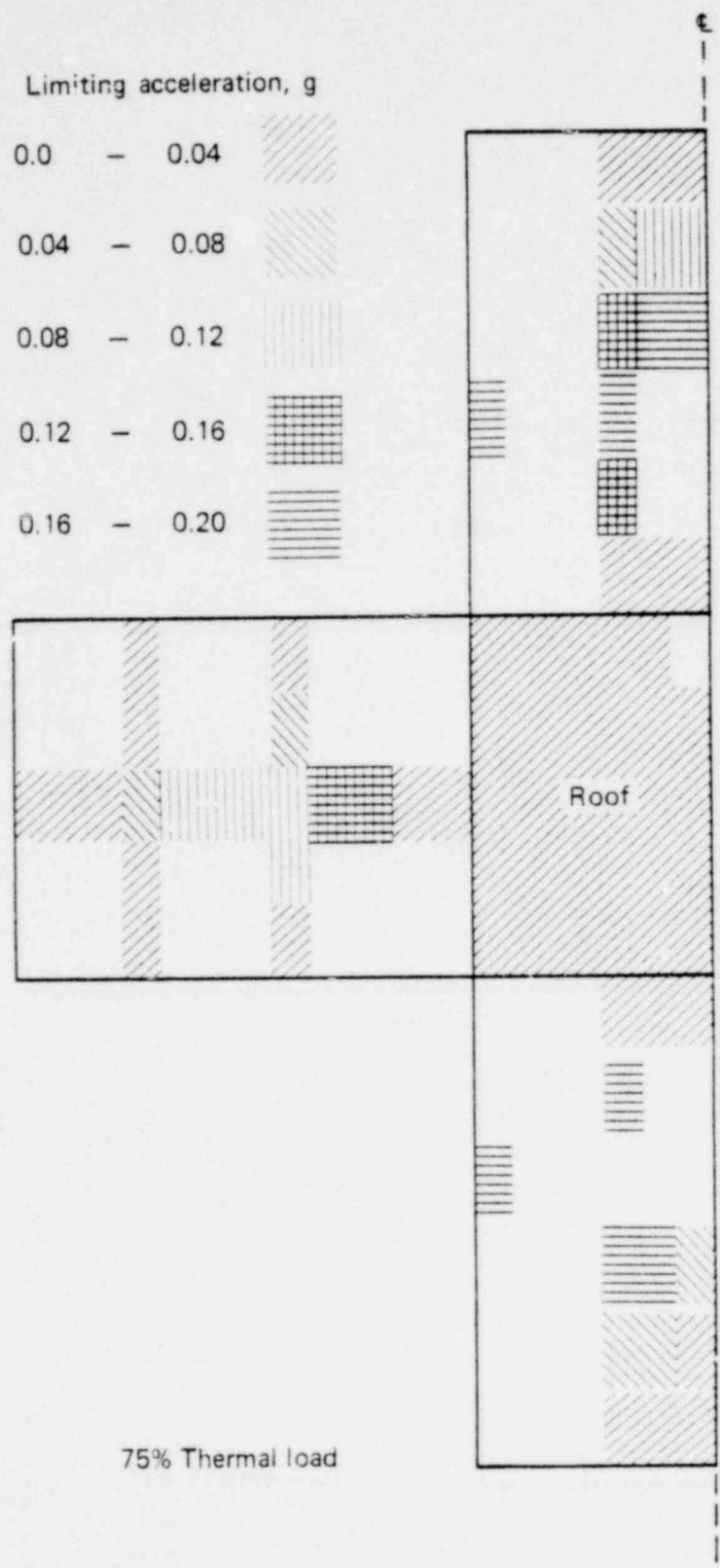


FIG. 12. Regions of vault model where limiting criteria are exceeded with 75% of the base thermal load included in the analysis.

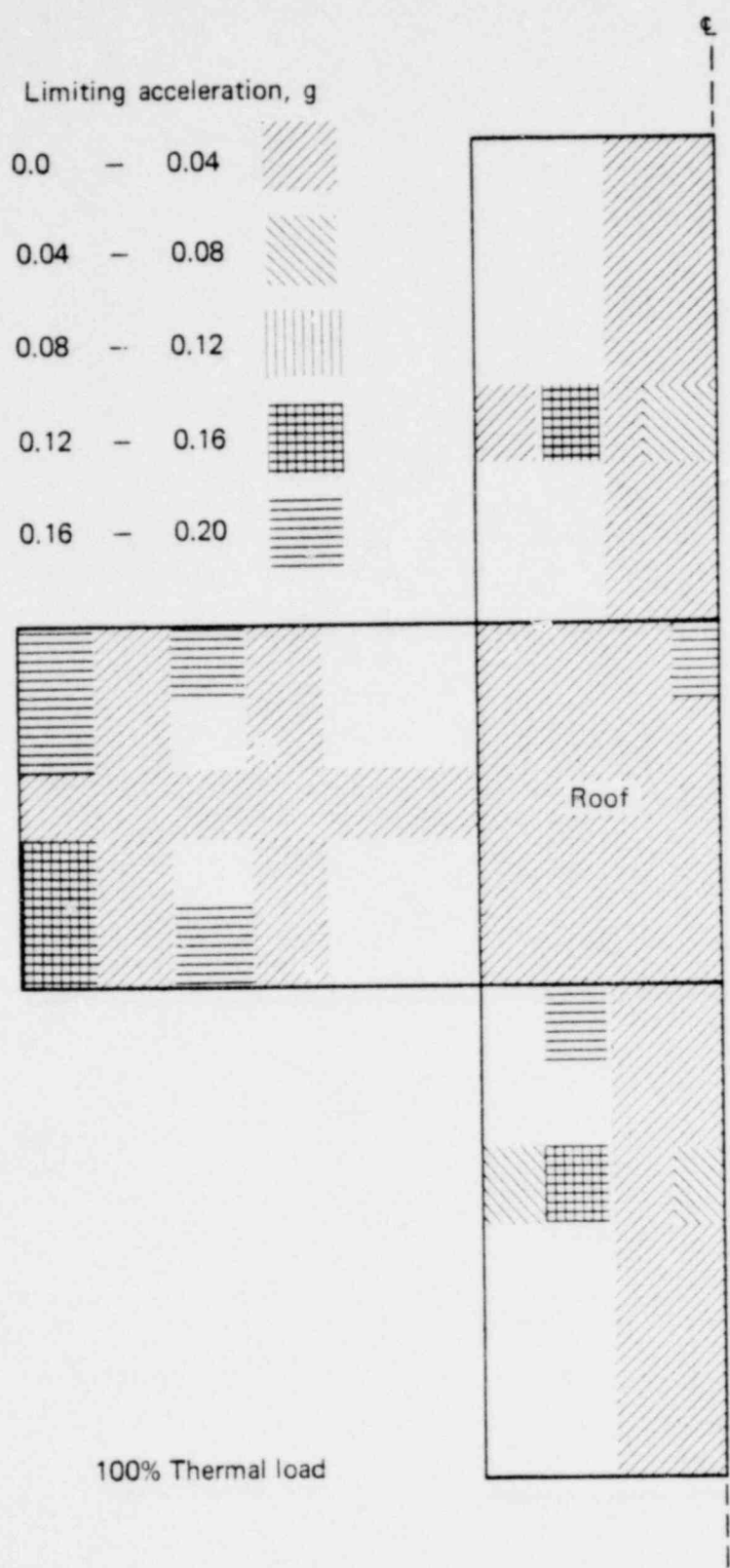


FIG. 13. Regions of vault model where limiting criteria are exceeded with 100% of the base thermal load included in the analysis.

285 585

CONCLUSIONS

Excluding any thermal load, both tanks and the vault have sufficient strength to sustain, without serious structural damage, ground excitations up to 0.2 g in addition to all mechanical loads, including dead load and pressure loads. The steel tanks have little thermal load and any thermal stress in them could be relieved by the bolt joints of the base plates. Consequently, the waste storage tanks are considered able to survive ground excitations with peak acceleration up to 0.2 g even though the base plates of the tank legs may yield locally.

The reinforced concrete vault, however, cannot relieve its thermal loads completely. The actual residual thermal stresses in the concrete vault cannot be determined in this study because of the nonlinear behavior of reinforced concrete and insufficient knowledge of the actual thermal gradient through the concrete walls or roof. Elastic stresses were calculated for the base case of 70°F thermal gradient. Results indicate that the limiting criteria for the vault are exceeded at low accelerations if the thermal load is above 50% of the base case.

A nonlinear analysis of the thermal load case is probably necessary for gaining a precise understanding of the behavior of the vault under combined seismic and thermal loads. Without such an analysis, we must rely on engineering judgment to estimate the actual thermal stress level in the vault and the peak ground acceleration that the vault can sustain. It is our estimate that the thermal stress in the vault is about 25% of the elastic stress calculated for the 70°F thermal gradient. If this is in fact the state of stress in the vault, then a limited area near the center of the vault may exceed our limiting criteria during an earthquake with peak acceleration between 0.13 and 0.2 g.

Our best estimate of the actual thermal load was submitted to the NRC in a review draft of this report. The NRC then asked that an additional study be done to confirm the use of the 25% thermal load case. This additional study estimated the maximum steady-state temperature gradient through the vault walls. Two approaches were used as explained in the Appendix. The maximum temperature differential was calculated to be 25.5⁰F, and results from the two methods agreed closely. This separate analysis confirms our selection of the 25% thermal load case as representative of the actual thermal gradient through the vault walls. It does not, however, eliminate the uncertainty that results from using linear techniques to analyze the nonlinear behavior of concrete.

ACKNOWLEDGMENT

The authors wish to acknowledge the assistance of Robert Bernero, A. Thomas Clark, C. J. Haughney, C. Ross Chappell, and Ronald Clary of the U.S. Nuclear Regulatory Commission, Office of Nuclear Material Safety and Safeguards for providing guidance and support throughout this study.

We also appreciate the time spent by Dorothy Ng in developing the mesh for the vault model and by Garry Holman in conducting the additional thermal gradient analysis (Appendix) requested by the NRC.

Finally, we wish to thank Robert Johnson of EG&G, Inc., for compiling the text.

REFERENCES

1. R. Murray, T. Nelson, and A. Davito, Seismic Analysis of the Nuclear Fuel Service Reprocessing Plant at West Valley, New York, Lawrence Livermore Laboratory, Livermore, CA, Report UCRL-52266 (1977).
2. R. Murray, T. Nelson, and A. Davito, Seismic Analysis of the Nuclear Fuel Service Reprocessing Plant at West Valley, New York: Documentation, Lawrence Livermore Laboratory, Livermore, CA, Report UCID-17453 (1977).
3. A. Davito, R. Murray, T. Nelson, and D. Bernreuter, Seismic Analysis of High Level Neutralized Liquid Waste Tanks at the Western New York State Nuclear Service Center, West Valley, New York, Lawrence Livermore Laboratory, Livermore, CA, Report UCRL-52485 (1978).
4. R. G. Dong and S. M. Ma, Structural Analyses of the Fuel Receiving Station Pool At The Nuclear Fuel Service Reprocessing Plant, West Valley, New York, Lawrence Livermore Laboratory, Livermore, CA, Report UCRL 52575 (1978).
5. S. Sackett, SAP4 Manual, Lawrence Livermore Laboratory, Livermore, CA, Internal Memorandum MDG 78-14 (Feb. 1978).
6. U.S. Nuclear Regulatory Commission, Design Response Spectra for Seismic Design of Nuclear Power Plants, Washington, D. C., Regulatory Guide 1.60 (Dec. 1973).
7. N. Mononobe and H. Matsuo, "On the Determination of Earth Pressures During Earthquakes," in Proc. World Eng. Conf. 9, 176, (1929).
8. S. Okabe, "General Theory of Earth Pressure," J. Jap. Soc. Civil Eng. 12 (1), (1926).
9. U.S. Nuclear Regulatory Commission, Damping Values for Seismic Design of Nuclear Power Plants, Washington, D. C., Regulatory Guide 1.61 (Oct. 1973).
10. L. S. Jacobson, "Impulsive Hydrodynamics of Fluid Inside a Cylindrical Tank and of a Fluid Surrounding a Cylindrical Pier," Bull. Seis. Soc. of Am. 39, (1949).

11. D. P. Clough, Experimental Evaluation of Seismic Design Methods for Broad Cylindrical Tanks, University of California at Berkeley, Report EERC 77-10 (1977).
12. A. K. Chopra and C. Y. Liaw, "Earthquake Resistant Design of Intake-Outlet Towers," ASCE J. of the Struc. Div., 1349 (July 1975).
13. N. M. Newmark, Inelastic Design of Nuclear Reactor Structures and its Implications on Design of Critical Equipment, Fourth SMIRT Conference, San Francisco (1977).
14. H. B. Seed and R. V. Whitman, Design of Earth Retaining Structures for Dynamic Loads, ASCE Specialty Conference on Lateral Stresses in Ground Excitation of Earth-Retaining Structures, Ithaca, New York, (June 22-24, 1976).
15. H. Matsuo and S. O'Hara, "Lateral Earth Pressures and Stability of Quay Walls During Earthquakes," in Proc. 2nd World Conference on Earthquake Engineering 1, Japan, (1960).
16. F. Besio, L. Lazzori, and M. Porfido, On the Influence of Concrete Cracking in the Stress Distribution in Some Typical Structures, Paper J417, Fourth SMIRT Conference, San Francisco (1977).

RKJ/ej/ew

1792 291

APPENDIX: CALCULATION OF THE MAXIMUM TEMPERATURE
DIFFERENTIAL THROUGH THE VAULT WALLS

The problem of estimating the maximum steady-state temperature gradient through the vault walls (for the purpose of calculating thermal stresses) is solved using two different techniques. The first is based on the method of flux plotting.¹ This graphical technique can provide quick and useful solutions to two-dimensional steady-state heat conduction problems for which extreme accuracy is not important. By constructing a grid of heat-flow lines (streamlines) and isotherms (equipotential lines), a purely geometrical shape factor can be defined that reduces the two-dimensional problem to a one-dimensional representation.

The second method is a general analytic solution for closed rectangular parallelepiped shells with arbitrary wall thicknesses, having six isothermal inner surfaces and six isothermal outer surfaces at specified constant temperatures.² Derived from empirical conduction data, this method treats the heat flow at the corners of the vault more accurately.

Both techniques essentially reduce the given three-dimensional conduction problem to a one-dimensional representation, the first by considering two-dimensional planar sections of the vault, the second by treating the vault as a parallelepiped shell. Because a "worst-case" solution is sought, and because details about the ambient medium are sketchy, these techniques are considered to be adequate.

The problem was solved by considering the vault to be enclosed within a control volume (or, in the two-dimensional case, a control surface) with a uniform thickness of 6.0 feet, equal to the depth of the overburden above the vault. The outer surface of the control volume is assumed to have a constant temperature of 32^o F. This boundary condition represents completely frozen

IPS 5011

soil surrounding the vault, a worst-case condition. In each case (2D and 3D), the temperature at the outer wall of the vault was obtained by matching expressions for heat flux at the interface between the vault and the control volume.

Representative material properties for the soil are defined assuming dry earth.³ The dry earth density (87 pcf) is below that used for the seismic analysis (120 pcf); however, the deviation is not important since density is not used in the steady-state calculation.

FLUX PLOT METHOD

Figure A1 shows the two-dimensional vault and control surface used for the flux plot method. Figure A2 shows a corner of the model and the flux plot--heat flow lines and isotherms--for the corner.

In general, the heat flow, q , across the temperature difference in either soil or concrete can be described by

$$q = k\zeta\Delta T$$

where k is heat conductance. The shape factor, ζ , is defined as

$$\zeta = \frac{N_C}{N_R} .$$

where

N_C is the number of flow tubes

and

N_R is the number of temperature increments.

The soil and concrete are represented by similar flux plots which share a common boundary. Matching heat flux at this boundary implies

$$k_1\zeta_1(T_1-T_2) = k_2\zeta_2(T_2-T_\infty) .$$

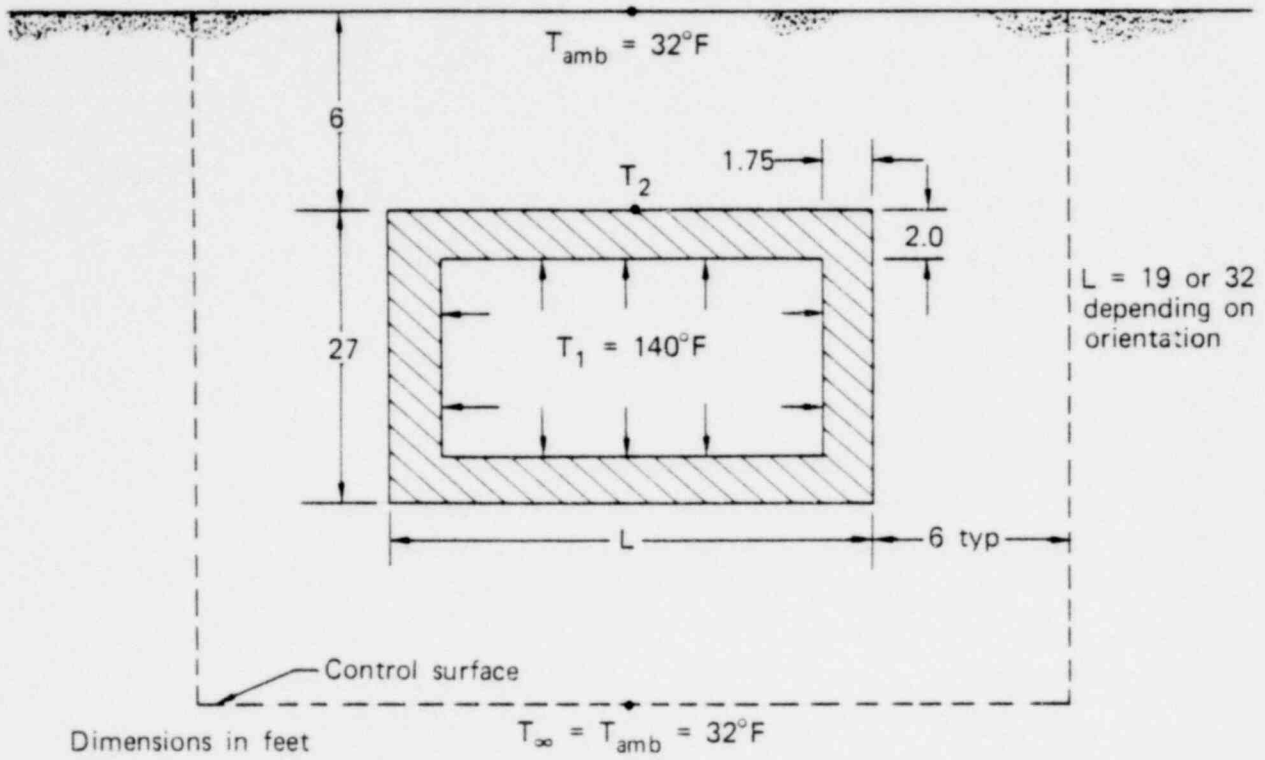


FIG. A1. Planar vault and control surface used for flux plot method.

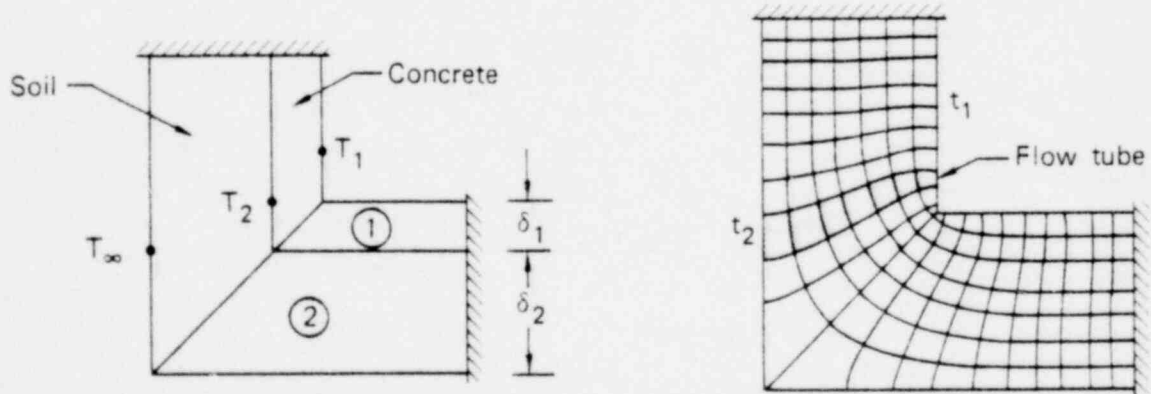


FIG. A2. Flux plot for a corner of the planar vault.

Because both regions share a common boundary and because the flux plot method requires that the aspect ratio of each cell in the net be ≈ 1 , this equation can be rewritten as

$$\frac{k_1}{\delta_1} (T_1 - T_2) = \frac{k_2}{\delta_2} (T_2 - T_\infty) .$$

Solving for T_2 in terms of T_1 and T_∞

$$T_2 - T_\infty = (T_1 - T_\infty) \left[\frac{\delta_2/k_2}{\delta_1/k_1 + \delta_2/k_2} \right] .$$

This equation was solved using $k_1 = 1$ Btu/hr-ft- $^{\circ}$ F and $k_2 = 0.85$ Btu/hr-ft- $^{\circ}$ F. Results of the calculation appear in Table A1.

TABLE A1. Results of flux plot calculations for T_2 and ΔT .

δ_2 , ft	T_∞ , $^{\circ}$ F	δ_1 , ft	T_2 , $^{\circ}$ F	$\Delta T = T_1 - T_2$, $^{\circ}$ F
6	32	1.75	118.5	21.5
		2.0	116.2	23.8
6	50	1.75	122.1	17.9
		2.0	120.8	19.2
12	32	1.75	128.1	11.9
		2.0	126.6	13.4

THREE DIMENSIONAL METHOD

Figure A3 shows the vault, control volume, and parameters used for this approach. In general,

$$q = K\Delta T$$

where K is an equivalent heat conductance calculated for the three-dimensional body. For the concrete enclosure

$$q = K_1(T_1 - T_2)$$

and for the soil control volume

$$q = K_2(T_2 - T_\infty).$$

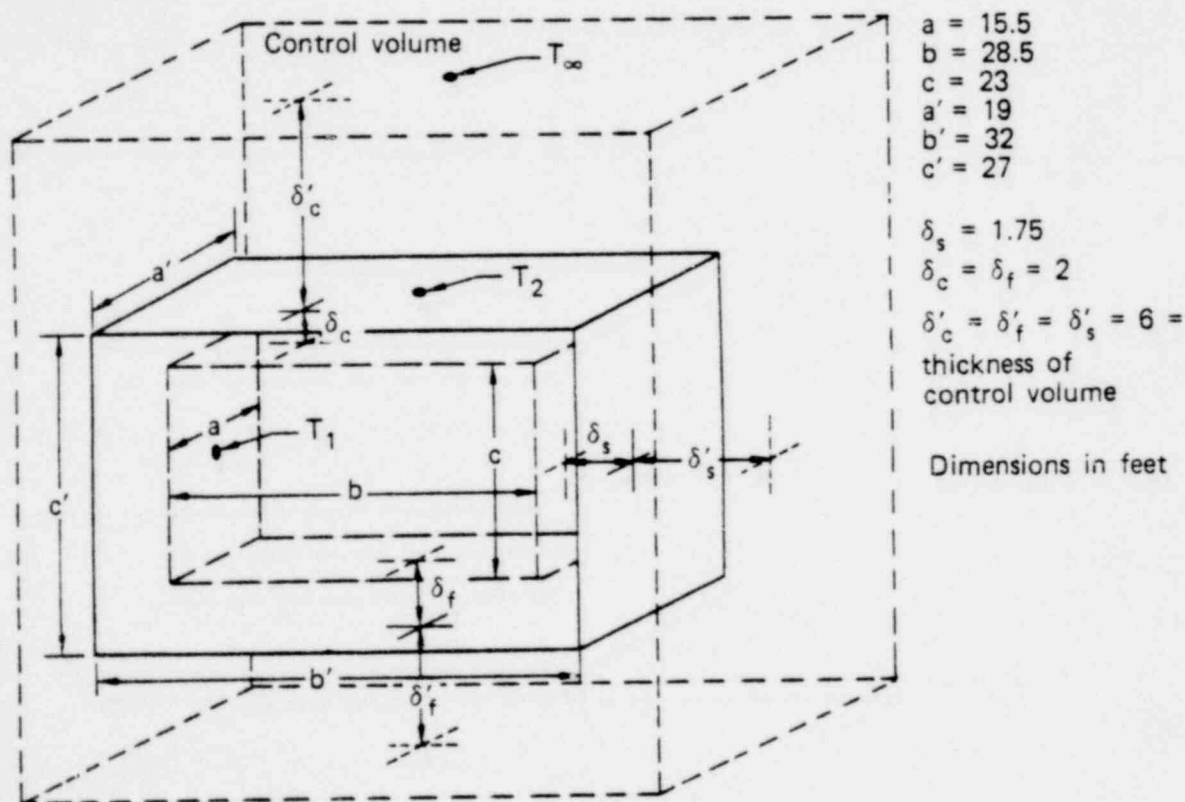


FIG. A3. Vault, control volume and geometric parameters for three-dimensional approach.

Matching fluxes implies

$$K_1(T_1 - T_2) = K_2(T_2 - T_\infty)$$

Solving for T_2 ,

$$T_2 - T_\infty = (T_1 - T_\infty) \left[\frac{1/K_2}{1/K_1 + 1/K_2} \right]$$

From geometric considerations,

$$\begin{aligned} K_1 &= k_1 \left[\frac{4ac}{\delta_s} + ab \left(\frac{1}{\delta_f} + \frac{1}{\delta_c} \right) + 1.08(a+b) + 2.16(a+c) + \right. \\ &\quad \left. 0.4(4\delta_s + \delta_f + \delta_c) \right] \\ &= 1392 \text{ Btu/hr-}^\circ\text{F} . \end{aligned}$$

Similarly,

$$K_2 = k_2 \left[\frac{S_1}{\delta} + 2.16(a' + b' + c') + 1.20\delta \right]$$

where

$$S_1 = 2(a'b' + b'c' + c'a')$$

$$\delta = \delta'_c = \delta'_f = \delta'_s .$$

Using the values in Fig. A3,

$$K_2 = 431 \text{ Btu/hr-}^\circ\text{F} .$$

Therefore,

$$\begin{aligned}T_2 - T_\infty &= (T_1 - T_\infty) \frac{1/431}{1/431 + 1/1392} \\ &= 82.5^\circ\text{F} \\ T_2 &= 114.5^\circ\text{F} \\ \Delta T &= T_1 - T_2 = 25.5^\circ\text{F}\end{aligned}$$

and $(\Delta T/\delta)_{\max} = 25.5/1.75 = 14.6^\circ\text{F}/\text{ft}$, which compares with a $(\Delta T/\delta)_{\max}$ of $13.6^\circ\text{F}/\text{ft}$ for the flux plot approach.

If T_∞ is increased to 50°F , ΔT is reduced to about 21.6°F . If T_∞ is held at 32°F and the thickness of the control volume is increased to 12 ft (except for the depth of overburden which remains at 6 ft), $K_2 = 428 \text{ Btu}/\text{hr}\text{-}^\circ\text{F}$, $T_2 = 114.5^\circ\text{F}$, and $\Delta T = 25.5^\circ\text{F}$.

RESULTS AND CONCLUSIONS

For the planar case, two analyses were completed for wall thicknesses of 1.75 ft and 2.0 ft, yielding temperature differentials through the wall of 21.5°F and 23.8°F , respectively. This result is independent of the orientation of the planar section taken through the vault because the geometric shape factors drop out of the calculation of the temperature at the vault-control volume interface.

Solution of the problem using the general parallelepiped relationship yielded a temperature differential of 25.5°F , only slightly higher than that predicted using the flux plot method. This result is taken as the "final" result, not only because it is more conservative, but also because the parallelepiped relationship, being derived from empirical heat conduction data, is expected to more accurately represent the actual three-dimensional vault. It is encouraging to note that the results of the two different types of analysis compare as closely as they do.

Companion analyses using the parallelepiped relationship were also performed for an ambient temperature of 50⁰F. In this case, the temperature differential through the walls of the vault is reduced to 21.6⁰F.

Calculations were also performed to determine the effect of the thickness of the control volume. It was determined through these calculations that the depth of the overburden above the vault is the controlling factor in the analysis, so long as the thickness of the control volume is at least equal to the depth of burial. If, for example, the thickness of the control volume is increased to 12 ft, except for the thickness of the overburden, the calculated temperature differential through the vault walls is essentially unchanged from the previous result.

In light of the constraints of time and the lack of detailed problem definition, these results appear to be reasonable estimates of the worst-case temperature differential that would occur in the walls of the concrete vault. It is emphasized, however, that more detailed calculations, including finite-element modeling, will be required if further quantification is desired.

APPENDIX REFERENCES

1. Eckert, E. R. G. and Drake, R. M., Analysis of Heat and Mass Transfer (McGraw-Hill Book Co., New York, 1973).
2. Rohsenow, W. M. and Hartnett, J. P., Handbook of Heat Transfer (McGraw-Hill Book Co., New York, 1973).
3. Bolz, R. E. and Tuve, G. L., Handbook of Tables for Applied Engineering Science (Chemical Rubber Co. Press, Cleveland, 1970) p. 133.

Distribution:

Docket File 50-201

~~POP~~ DCS

LPDR

RM 50-6

NMSS R/F

FCAF R/F

WJDircks

RECunningham

TFCarter

JBMartin

MJBell

JMalaro

PLohaus

Streby

DSwanson

RBlack

JGray

IE:HQ (3)

JShafer

ATClark

EMcCarthy

TElsasser

CJHaughney

FPang, GAO

ECTonti

GDCalkins

AAbriss

DSmith

JShafer

bcc: Distribution List

DISTRIBUTION LIST

October 5, 1979

NUCLEAR FUEL SERVICES, INC.
WEST VALLEY, NEW YORK

Richard Lester
Research Associates
1137 Avenue of the Americas
New York, N. Y. 10036

Mr. Sherwood Davies
Bureau of Radiological Health
Tower Building
Empire State Plaza
Albany, New York 12237

County Clerk
303 Court Street
Cattaraugus County
Little Valley, N.Y. 14755

Supervisor, Town of Ashford
135 Depot Street
West Valley, N.Y. 14171

Director, Technical Develop-
ment Programs
State of New York Energy
Office
Agency Building 2
Empire State Plaza
Albany, New York 12223

N.Y. State Department of
Environmental Conservation
ATTN: Director
Office of Environmental
Analysis
Albany, N.Y. 12201

U.S. Environmental Pro-
tection Agency
ATTN: EIS Coordinator
Region II Office
26 Federal Plaza
New York, N.Y. 10007

Dr. Robert Fakundiny
N.Y. State Geological Survey
Rm. 973, State Education
Building Annex
Albany, N.Y. 12234

T. B. Hindman
High Level Waste Project
Office
Savannah River Operations
Office
P. O. Box A
Aiken, SC 29801

Dr. Marvin Resnikoff, Chmn.
Energy Task Force
Sierra Club, Niagara Group
Box 64, Station G
Buffalo, N.Y. 14213

Natural Resources Defense Co.
917 15th Street, N.W.
Washington, D. C. 20005

Joan Loring, Esq.
Assistant County Attorney
County of Erie
25 Delaware Avenue
Buffalo, N. Y. 14202

Louis J. Lefkowitz, Esq.
Attorney General of the
State of New York

ATTN: Richard G. Berger,
Deputy Asst. Attorney
General
Two World Trade Center
New York, N. Y. 10047

The Honorable Stanley N. Lundine
U.S. House of Representatives
ATTN: Mary Ann Richardson
Washington, D.C. 20515

J. Richardson Lippert, II, Esq.
18 South Main Street
Franklinville, N.Y. 14737

John Henry Schlegel, Esq.
32 South Drive
Buffalo, N.Y. 14226

Mr. Edward Wagoner
Citizens' Energy Council of
Western New York
P. O. Box 312
Wilson, N. Y. 14172

C. J. Clementi, Esq.
Special Counsel
N.Y. State Energy Research
and Development Authority
Rockerfeller Plaza
Agency Building 2
Albany, N. Y. 12223

Mr. David Berick
Environmental Policy Center
317 Pennsylvania Avenue, S. E.
Washington, D. C. 20003

William E. Straub, Esq.
First Asst. County Atty.
County of Erie
25 Delaware Avenue
Buffalo, N.Y. 14202

Mr. Ross Scott
102 Heath Street
Buffalo, N. Y.

Butzel & Kass
45 Rockerfeller Plaza
New York, N. Y. 10020

The Honorable William B. Hoyt
Chairman
Legislative Commission on Science
and Technology
State of New York
13th Floor, Agency Building 4
Assembly P. O. Box 167
Albany, N. Y. 12248

Maurice Axelrad, Esq.
Lowenstein, Newman, Reis,
& Axelrad
1025 Connecticut Ave., N.W.
Washington, D.C. 20036

Mr. Neil J. Newman
Nuclear Fuel Services
6000 Executive Blvd.
Rockville, Md. 20852

Dr. Charles Luner
Argonne National Laboratory
9700 South Cass Avenue
Argonne, Illinois 60439

Carl Mongerson
10734 Sharp Street
East Concord, N.Y. 14055

Mr. David McGoff
Chief, Projects Branch
Division of Waste Management
Department of Energy
Germantown, Md. MS B-107

1792 302



UNITED STATES
NUCLEAR REGULATORY COMMISSION
WASHINGTON, D. C. 20555

DEC 19 1979

Docket No. 50-201

MEMORANDUM FOR: Leland C. Rouse, Chief
Advanced Fuel and Spent Fuel Licensing Branch

FROM: A. T. Clark, Jr. and Charles J. Haughney
Advanced Fuel and Spent Fuel Licensing Branch

SUBJECT: MEETING WITH NUCLEAR FUEL SERVICES, INC. (NFS) ON
EFFECT OF TORNADO ON DORMANT PLANT AT WEST VALLEY, NEW YORK

The subject meeting was held on December 10, 1979 at NRC offices in Silver Spring, Maryland. A list of attendees is attached. The purpose of the meeting was to describe and discuss the analysis performed for or by the Nuclear Regulatory Commission on the effect of tornado on the dormant reprocessing plant at West Valley, New York. The topics covered are shown in Attachment 2.

Mr. Abbey, of the NRC Office of Regulatory Research, discussed the results of analyses conducted by Dr. Fujita of the University of Chicago and Dr. MacDonald of Texas Technical Institute. Each analysis determined the relationship between tornado size and recurrence interval. The viewgraphs presented are not reproducible for this meeting summary. However, both researchers had very close agreement as approximately indicated on Table 1 below.

Table 1

Tornado Probabilities

<u>Maximum Windspeed</u>	<u>Annual Probability</u>
100	5×10^{-4}
200	5×10^{-7}
300	10^{-9}

1792 303